Li, H., Rodrat, M., Al Salmani, M. K. A., Veselu, D., Han, S., Raraigh, K., Cutting, G., & Sheppard, D. N. (2024). Two rare variants that affect the same amino acid in CFTR have distinct responses to ivacaftor. *Journal of Physiology*, *602*(2), 333-354. https://doi.org/10.1113/JP285727

Peer reviewed version

License (if available):
CC BY

Link to published version (if available):
10.1113/JP285727

Link to publication record in Explore Bristol Research
PDF-document

This is the accepted author manuscript (AAM) of the article which has been made Open Access under the University of Bristol's Scholarly Works Policy. The final published version (Version of Record) can be found on the publisher's website. The copyright of any third-party content, such as images, remains with the copyright holder.

University of Bristol - Explore Bristol Research
General rights

This document is made available in accordance with publisher policies. Please cite only the published version using the reference above. Full terms of use are available:
http://www.bristol.ac.uk/red/research-policy/pure/user-guides/ebr-terms/

TWO RARE VARIANTS THAT AFFECT THE SAME AMINO ACID IN CFTR HAVE DISTINCT RESPONSES TO IVACAFTOR

Hongyu Li[1 *], Mayuree Rodrat[1,2 *], Majid K. Al-Salmani[1,3], Diana-Florentina Veselu[4], Sangwoo T. Han[5], Karen S. Raraigh[5], Garry R. Cutting[5] and David N. Sheppard[1]

[1] Schools of Physiology, Pharmacology and Neuroscience and [4] Biochemistry, University of Bristol, Bristol, UK,

[2] Center of Research and Development for Biomedical Instrumentation, Institute of Molecular Biosciences, Mahidol University, Nakhon Pathom, Thailand,

[3] Department of Physiology, College of Medicine and Health Sciences, Sultan Qaboos University, Al Khoudh, Muscat, Sultanate of Oman

and

[5] Department of Genetic Medicine, Johns Hopkins University School of Medicine, Baltimore, Maryland, USA

Running Title: Distinct effects of ivacaftor on two rare variants in CFTR

Key Words: CFTR chloride ion channel; cystic fibrosis; rare variant; ivacaftor (VX-770); CFTR potentiation; CFTR inhibition

Total Number of Words: 7,410 words, excluding references and figure legends

Table of Contents Category: Molecular and Cellular

Author contributions: *HL and MR are co-first author

Address Correspondence to: D.N. Sheppard, PhD
University of Bristol
School of Physiology, Pharmacology and Neuroscience
Biomedical Sciences Building
University Walk
Bristol BS8 1TD
United Kingdom
Tel: +44 117 455 2316
E-mail: D.N.Sheppard@bristol.ac.uk

KEY POINTS SUMMARY

- Dysfunction of the ion channel cystic fibrosis transmembrane conductance regulator (CFTR) causes the genetic disease cystic fibrosis (CF).
- This study investigated two rare pathogenic *CFTR* variants, S1159F and S1159P, which affect the same amino acid in CFTR to understand the molecular basis of disease and response to the CFTR-targeted therapy ivacaftor.
- Both rare variants diminished CFTR function by modestly reducing current flow through the channel and severely inhibiting ATP-dependent channel gating with S1159F exerting the stronger adverse effect, which correlates with its association with more severe disease.
- Ivacaftor potentiated channel gating by both rare variants without restoring their activity to wild-type levels, but concurrently reduced current flow through open channels, particularly those of S1159F-CFTR.
- Our data demonstrate that S1159F and S1159P cause CFTR dysfunction by multiple mechanisms that require combinations of CFTR-targeted therapies to fully restore channel function.

ABSTRACT

Some residues in the cystic fibrosis transmembrane conductance regulator (CFTR) channel are the site of more than one *CFTR* variant that cause cystic fibrosis. Here, we investigated the function of S1159F and S1159P, two variants associated with different clinical phenotypes, which affect the same pore-lining residue in transmembrane segment twelve that are both strongly potentiated by ivacaftor when expressed in CFBE41o$^-$ bronchial epithelial cells. To study the single-channel behaviour of CFTR, we applied the patch-clamp technique to Chinese hamster ovary cells heterologously expressing *CFTR* variants incubated at 27 °C to enhance channel residence at the plasma membrane. S1159F- and S1159P-CFTR formed Cl^- channels activated by cAMP-dependent phosphorylation and gated by ATP that exhibited thermostability at 37 °C. Both variants modestly reduced the single-channel conductance of CFTR. By severely attenuating channel gating, S1159F- and S1159P-CFTR reduced the open probability (P_o) of wild-type CFTR by ≥ 75% at ATP (1 mM); S1159F-CFTR caused the greater decrease in P_o consistent with its more severe clinical phenotype. Ivacaftor (10 – 100 nM) doubled the P_o of both *CFTR* variants without restoring P_o values to wild-type levels, but concomitantly, ivacaftor decreased current flow through open channels. For S1159F-CFTR, the reduction of current flow was marked at high (supersaturated) ivacaftor concentrations (0.5 – 1 μM) and voltage-independent, identifying an additional detrimental action of elevated ivacaftor concentrations. In conclusion, S1159F and S1159P are gating variants, which also affect CFTR processing and conduction, but not stability, necessitating the use of combinations of CFTR modulators to optimally restore their channel activity.

ABBREVIATIONS

CF, cystic fibrosis; CFTR, cystic fibrosis transmembrane conductance regulator; *i*, single-channel current amplitude; IBI, interburst interval; M, transmembrane segment; MBD, mean burst duration; MSD, membrane-spanning domain; NBD, nucleotide-binding domain; P_o, open probability; PKA, protein kinase A

INTRODUCTION

Cystic fibrosis transmembrane conductance regulator (CFTR) modulators have transformed the treatment of the genetic disease cystic fibrosis (CF) (Ramsey *et al*., 2011; Heijerman *et al*., 2019; Middleton *et al*., 2019). These drugs target the root cause of CF, pathogenic variants in the epithelial anion channel CFTR, not just in the respiratory airways, the major site of disease, but in all affected organs (Ratjen *et al*., 2015; Yeh *et al*., 2022). Although most people with CF carry one or two copies of the predominant *CFTR* variant, c.1521_1523delCTT (p.Phe508del; legacy: F508del) (Cutting, 2015), over 2,100 sequence variations have been reported in the *CFTR* gene (http://www.genet.sickkids.on.ca/), of which approximately 800 have been thoroughly vetted (https://cftr2.org/). To ensure that CFTR modulators reach as many people with CF as possible, *CFTR* variants are grouped into theratypes based on (i) their impact on the synthesis, plasma membrane stability and function of CFTR and (ii) their response to CFTR modulators (Cutting, 2015).

Highlighting their importance for CFTR structure and function, some residues in CFTR are the site of more than one *CFTR* variant. One such residue is the serine at codon 1159 in the twelfth transmembrane segment (M12) that is part of membrane-spanning domain 2 (MSD2). Two rare missense substitutions are found at codon 1159: c.3476C>T (p.Ser1159Phe; legacy: S1159F) replaces the polar serine residue by the non-polar residue phenylalanine, whereas c.3475T>C (p.Ser1159Pro; legacy: S1159P) introduces the helix breaker proline (Fig. 1). For several reasons, we were keen to investigate these *CFTR* variants. First, they affect a pore-lining residue, which interacts with anions flowing through the CFTR channel (Hwang *et al*., 2018). Second, although the number of people with CF and S1159-*CFTR* variants is small, the two variants appear to bestow different disease phenotypes. S1159P appears to confer a non-classical clinical phenotype, demonstrated by its more common association with pancreatic sufficiency, lower mean sweat chloride concentration and the older average age of people with this variant, whereas S1159F likely confers a classical clinical phenotype expounded by its association with pancreatic insufficiency (Table 1) (Knowles & Durie, 2002) (https://cftr2.org/). However, no difference in CFTR-mediated transepithelial Cl^- current was observed when the two S1159-*CFTR* variants were heterologously expressed in the immortalized human CF bronchial epithelial cell line CFBE41o$^-$ and studied with the Ussing chamber technique (Han *et al*., 2018). Third, S1159F- and S1159P-CFTR-expressing CFBE41o$^-$ epithelia exhibited a notable response to the CFTR potentiator ivacaftor (Han *et al*., 2018). Among 59 *CFTR* variants investigated,

S1159F- and S1159P-CFTR were classified with the *CFTR* gating variant c.1652G>A (p.Gly551Asp; legacy G551D) as high responders based on the magnitude of the increase in CFTR-mediated transepithelial Cl^- current achieved with ivacaftor (Han *et al*., 2018).

Therefore, we were interested to learn how S1159-*CFTR* variants affect the properties and regulation of the CFTR Cl^- channel and its response to ivacaftor. To address these aims, we heterologously expressed the S1159-*CFTR* variants in Chinese hamster ovary (CHO) cells and studied their single-channel behaviour in cell-free membrane patches with the patch-clamp technique. We discovered that both S1159-*CFTR* variants modestly reduced current flow through CFTR, but markedly attenuated channel gating with S1159F causing the harsher impact. Low nanomolar concentrations of ivacaftor doubled the activity of S1159F- and S1159P-CFTR without achieving wild-type levels of activity, while higher (supersaturated) concentrations of ivacaftor caused voltage-independent inhibition of current flow through S1159F-CFTR. We conclude that S1159-*CFTR* variants cause conduction and gating defects that are partially rescued by ivacaftor. S1159F more severely impacts CFTR function consistent with its association with classical CF.

METHODS

Cells and CFTR expression

For single-channel studies of human *CFTR* variants, we used Chinese hamster ovary K1 (CHO-K1) cells (cat no. CCL-61, RRID:CVCL_0214; ATCC, Manassas, VA, USA). They were cultured in Ham's F-12 nutrient medium (cat no. 21765-029) supplemented with 10% fetal bovine serum (cat no. 26140-087), 100 U ml^{-1} penicillin and 100 μg ml^{-1} streptomycin (cat no. 15140-122) [all from Invitrogen (now Thermo Fisher Scientific), Paisley, UK] at 37 °C in a humidified atmosphere of 5% CO_2. CHO-K1 cells seeded on glass coverslips were co-transfected with *CFTR* variants and enhanced green fluorescent protein N1 (eGFP-N1, RRID:Addgene_172281) using the Lipofectamine 3000 system (cat no. L3000-001; Thermo Fisher Scientific). To increase the plasma membrane expression of S1159-*CFTR* variants, CHO cells were incubated at 27 °C for 7 – 12 days prior to study, changing media every second day (Denning *et al*., 1992). Then, GFP-expressing CHO-K1 cells were selected for study using the patch-clamp technique.

In some single-channel studies, control data were acquired from mouse mammary epithelial (C127) cells (RRID:CVCL_6550) stably expressing wild-type human CFTR [gift of

C.R. O'Riordan (Sanofi Genzyme)] (Marshall *et al*., 1994). These cells were cultured and used as described previously (Sheppard & Robinson, 1997). C127 cells are the cell line of choice for single-channel studies of wild-type human CFTR because they express low levels of heterologously expressed CFTR (Sheppard & Robinson, 1997). Under the experimental conditions used, the single-channel behaviour of human CFTR in excised inside-out membrane patches from different mammalian cells is equivalent (Lansdell *et al*., 1998; Chen *et al*., 2009; Bose *et al*., 2019).

Patch-clamp experiments

CFTR Cl^- channels were recorded in excised inside-out membrane patches using an Axopatch 200B patch-clamp amplifier and pCLAMP software (version 10.4, RRID:SCR_011323) (both from Molecular Devices, San Jose, CA, USA) (Cai *et al*., 2015). Unless otherwise indicated, the pipette (extracellular) solution contained (mM): 140 *N*-methyl-D-glucamine (NMDG), 140 aspartic acid, 5 $CaCl_2$, 2 $MgSO_4$ and 10 *N*-tris[hydroxymethyl]methyl-2-aminoethanesulphonic acid (TES), adjusted to pH 7.3 with Tris ([Cl^-], 10 mM). The bath (intracellular) solution contained (mM): 140 NMDG, 3 $MgCl_2$, 1 CsEGTA and 10 TES, adjusted to pH 7.3 with HCl ([Cl^-], 147 mM; free [Ca^{2+}], $< 10^{-8}$ M). Using a temperature-controlled microscope stage (Brook Industries, Lake Villa, IL, USA), the temperature of the intracellular solution was maintained at 37 °C.

Within two minutes of membrane patch excision, we added the catalytic subunit of protein kinase A (PKA; 75 nM) and ATP (1 mM) to the intracellular solution to activate CFTR Cl^- channels. Wild-type CFTR Cl^- channels were activated at 37 °C, but those of S1159F- and S1159P-CFTR were activated at 23 °C before raising the temperature of the intracellular solution to 37 °C once channel activation was complete. To minimise channel rundown, we added PKA (75 nM) to all intracellular solutions, maintained the ATP concentration at 1 mM unless investigating the ATP dependence of channel gating and clamped voltage at –50 mV. The effects of ivacaftor were studied by acquiring 3 – 8 min of single-channel data once channel activity stabilised following its addition to the intracellular solution in the continuous presence of PKA (75 nM) and ATP (1 mM). Because of the difficulty of washing ivacaftor from the recording chamber (Wang *et al*., 2014), test interventions with ivacaftor were not compared with pre- and post-intervention control periods. Instead, they were compared with the pre-intervention control period made with the same concentration of PKA and ATP, but without ivacaftor. To investigate the action of

ivacaftor at different voltages, we used symmetrical Cl^--rich solutions and stepped voltage from 0 mV to ±60 mV in 20 mV increments of 60 s at negative voltages, but 30 s duration at positive voltages. We chose 30 s voltage steps at positive voltages because this time interval was long enough to acquire sufficient transitions to quantify open probability (P_o), but short enough to prevent seal breakdown and loss of excised inside-out membrane patches. We did not step voltage to voltages beyond ±60 mV because of the weak inward rectification of wild-type human CFTR Cl^- currents at large positive voltages (Cai *et al*., 2003).

In this study, we used excised inside-out membrane patches containing ≤ 5 active channels [wild-type CFTR, number of active channels (N) ≤ 4; S1159F-CFTR, ≤ 5; S1159P-CFTR, ≤ 5]. To determine channel number, we used the maximum number of simultaneous channel openings observed during an experiment (Cai *et al*., 2006). To minimise errors, we used experimental conditions that robustly potentiated channel activity and verified that recordings were of sufficient length to determine the correct number of channels (Venglarik *et al*., 1994). Despite our precautions, we cannot exclude the possibility of unobserved S1159F- and S1159P-CFTR Cl^- channels in excised membrane patches. Therefore, P_o values for S1159-*CFTR* variants might possibly be overestimated.

Single-channel currents were acquired directly to computer hard disc after filtering at a corner frequency (f_c) of 500 Hz using an eight-pole Bessel filter (model F-900C/9L8L, Frequency Devices Inc., Ottawa, IL, USA) and digitising at a sampling rate of 5 kHz using a DigiData 1440A interface (Molecular Devices) and pCLAMP software (version 10.4). To measure single-channel current amplitude (i), Gaussian distributions were fit to current amplitude histograms. Using i values at negative voltages, we calculated single-channel conductance where the single-channel current-voltage relationship is linear in the presence of a large Cl^- concentration gradient (Fig. 4*B*) (Sheppard *et al*., 1993). For P_o measurements, lists of open- and closed-times were generated using a half-amplitude crossing criterion for event detection and dwell time histograms constructed as previously described (Sheppard & Robinson, 1997); transitions < 1 ms were excluded from the analysis [eight-pole Bessel filter rise time ($T_{10\text{-}90}$) ~0.73 ms at f_c = 500 Hz]. Histograms were fitted with one or more component exponential functions using the maximum likelihood method. For burst analyses, we used a t_c (the time that separates interburst closures from intraburst closures) determined from closed time histograms [wild-type CFTR, t_c = 13.3 ± 2.4 ms (n = 4); S1159F-CFTR, t_c = 21.5 ± 6.3 ms (n = 15); S1159P-CFTR, t_c = 21.8 ± 5.9 ms (n = 13) determined in the presence

of ATP (1 mM)] (Cai *et al*., 2006). The mean interburst interval (T_{IBI}) was calculated using the equation (Cai *et al*., 2006):

$$P_o = T_b / (T_{MBD} + T_{IBI}), \qquad \text{(Eq. 1)}$$

where, T_b = (mean burst duration) x (open probability within a burst). Mean burst duration (T_{MBD}) and open probability within a burst ($P_{o(burst)}$) were determined directly from experimental data using pCLAMP software. Only membrane patches that contained a single active channel were used for burst analyses. For illustration purposes, single-channel records were filtered at 500 Hz and digitised at 5 kHz before file size compression by 5-fold data reduction.

Reagents

PKA purified from bovine heart (cat no. 539576-25UG) was purchased from Calbiochem (now Merck Life Science UK Ltd.) (Gillingham, UK). Ivacaftor (cat no. S1144) was obtained from Selleck Chemicals (Stratech Scientific Ltd., Newmarket, UK), while all other chemicals, including ATP (disodium salt) (cat no. A2383-1G) and TES (cat no. T1375-500G) were supplied by Sigma-Aldrich Ltd. (now Merck Life Science UK Ltd.).

Stock solutions of ATP were prepared in intracellular solution directly before each experiment. Ivacaftor stock solutions were solubilised in DMSO before storage at –20 °C. Immediately before use, stock solutions were diluted to final concentrations with intracellular solution and, where necessary, the pH of the intracellular solution was readjusted to pH 7.3 to avoid pH-dependent changes in CFTR function (Chen *et al*., 2009). DMSO was without effect on the single-channel activity of CFTR (Sheppard & Robinson, 1997). On completion of experiments, the recording chamber was thoroughly cleaned before re-use (Wang *et al*., 2014).

Modelling

Using the atomic structure of phosphorylated ATP-bound human CFTR complexed with ivacaftor (PDB id: 6O2P; Liu *et al*., 2019), we investigated the impact of the rare *CFTR* variants at codon 1159 in M12 on CFTR structure. Figure 1 was made using PyMOL software (version 2.3.0) (RRID:SCR_000305).

Statistics

Data recording and analyses were randomised, but not blinded. To avoid pseudo-replication, all experiments were repeated at different times. Results are expressed as means ± SD of *n* observations, where *n* represents the number of individual excised inside-out membrane patches obtained from different cells from either ≥ 5 transfections for S1159-*CFTR* variants or ≥ 4 passages of cells for wild-type CFTR. However, some group sizes were unequal due to technical difficulties with the acquisition of single-channel data. All data were tested for normal distribution using a Shapiro-Wilk normality test. To test for differences between two groups of data acquired within the same experiment, we used Student's paired t-test. To test for differences between multiple groups of data, we used one-way, repeated measures analysis of variance (ANOVA) followed by either Dunnett's or Tukey multiple comparison test when a statistically significant difference was observed. Data subjected to statistical analyses had *n* values ≥ 5 per group. Tests were performed using SigmaPlot (version 14.0, RRID:SCR_003210; Systat Software Inc., San Jose, CA). Differences were considered statistically significant when $P < 0.05$.

RESULTS

S1159-*CFTR* variants perturb the single-channel conductance and gating behaviour of CFTR

In this study, we investigated the impact on human CFTR function and response to ivacaftor of two rare *CFTR* variants S1159F and S1159P, which affect the same pore-lining residue in M12 (Fig. 1). To study these *CFTR* variants, we used transiently transfected CHO cells incubated at 27 °C for ≥ 7 days to promote the plasma membrane expression of CFTR. With the patch-clamp technique, we examined the properties and regulation of CFTR Cl^- channels and the action of ivacaftor.

Figure 2 and Figure 3*A* show representative multi- and single-channel recordings, respectively, of wild-type, S1159F- and S1159P-CFTR in excised inside-out membrane patches from CHO cells acquired at –50 mV with ATP (1 mM) and PKA (75 nM) in the intracellular solution. Consistent with previous results (Han *et al*., 2018), the multi-channel recordings, each acquired using membrane patches with four active channels, demonstrate that the S1159-*CFTR* variants diminished strongly CFTR activity (Fig. 2). Figure 3*A* reveals that S1159-*CFTR* variants attenuated the single-channel behaviour of CFTR in two important ways. First, S1159F and S1159P reduced current flow through open channels. At –50 mV in the presence of a large Cl^- concentration gradient ($[Cl^-]_{int}$, 147 mM; $[Cl^-]_{ext}$, 10 mM), the

single-channel current amplitude (*i*) of CFTR was reduced by 24 and 21% by S1159F and S1159P, respectively, (Fig. 3*A* and *B*). To further quantify the reduction in current flow, we constructed single-channel current-voltage (*i*-*V*) relationships and measured single-channel conductance. Using a large Cl^- concentration gradient, the *i*-*V* relationship of wild-type CFTR strongly inwardly rectifies, but at negative voltages, it is linear (Sheppard *et al*., 1993). Figure 4*A* shows representative single-channel recordings of wild-type, S1159F- and S1159P-CFTR at different membrane voltages using these experimental conditions, while Figure 4*B* presents the summary single-channel *i*-*V* relationships. At negative voltages, the calculated single-channel slope conductances of S1159F-CFTR (8.63 ± 0.55 pS; n = 3) and S1159P-CFTR (7.91 ± 1.46 pS; n = 7) were modestly reduced compared to that of wild-type CFTR (9.78 ± 0.81 pS; n = 6) (Fig. 4*C*).

Second, S1159F and S1159P disrupted the pattern of channel gating. The gating pattern of wild-type CFTR is characterized by bursts of channel openings interrupted by brief, flickery closures, separated by longer closures between bursts (Fig. 3*A*). Although both *CFTR* variants retained a bursting pattern of channel gating, the frequency of channel openings and their duration were greatly decreased. Burst analysis revealed that the interburst interval (IBI, the average duration of the long closures separating one open channel burst from the next) was increased by 637 and 460% for S1159F- and S1159P-CFTR, respectively, while mean burst duration (MBD, the average duration of an open channel burst) was reduced by 70 and 44% for S1159F- and S1159P-CFTR, respectively, using PKA (75 nM) and ATP (1 mM) (Fig. 3*A*, *C* and *D*). As a result, the P_o of CFTR was diminished 89 and 74% by S1159F and S1159P, respectively, (Fig. 3*E*).

To understand better the impact of the S1159-*CFTR* variants on CFTR channel gating, we investigated gating kinetics using membrane patches that contained only a single active CFTR Cl^- channel. Like those of wild-type CFTR, the open and closed time histograms of the S1159-*CFTR* variants were best fitted with one- and two-component exponential functions, respectively, (Fig. 5 and Table 2). The two populations of channel closures, described by fast (τ_{C1}) and slow (τ_{C3}) closed time constants, represented the brief, flickery closures that interrupt open channel bursts and the prolonged channel closures, which separate one open channel burst from the next (Table 2) (Sheppard & Robinson, 1997). Consistent with the analysis of bursts (Fig. 3*C* and *D*), Figure 5 and Table 2 suggest that the diminished P_o values of the S1159-*CFTR* variants were predominantly caused by lengthening of the slow closed

time constant (τ_{C3}) (S1159F, 514%; S1159P, 132%), although both variants also noticeably reduced the open time constant (τ_{O2}) (S1159F, 78%; S1159P, 68%). Figure 5 and Table 2 also reveal that the fast closed time constant (τ_{C1}) of the S1159-*CFTR* variants tended to be longer than that of wild-type CFTR, while its share of the closed time distribution was slightly decreased. Thus, the S1159-*CFTR* variants cause severe channel gating defects with S1159F-CFTR exerting the stronger effect.

S1159-*CFTR* variants disrupt channel gating by ATP

Following CFTR phosphorylation by PKA, channel gating is controlled by cycles of ATP binding and hydrolysis at the NBDs, which drive conformational changes in the MSDs that open and close the CFTR pore (Hwang *et al*., 2018). Therefore, we hypothesized that the defective channel gating of S1159-*CFTR* variants might reflect altered affinity and/or efficacy of channel gating by ATP. To test this idea, we examined the ATP-dependence of channel gating using excised membrane patches containing ≤ 4 active channels bathed in different ATP concentrations (0.03 – 3 mM) in the continuous presence of PKA (75 nM).

Figure 6*A* shows representative single-channel recordings of wild-type CFTR, S1159F- and S1159P-CFTR acquired at different intracellular ATP concentrations and Figure 6*B* summary P_o-ATP concentration relationships. Like that of wild-type CFTR, P_o values of the S1159-*CFTR* variants increased as the ATP concentration was elevated because IBI values decreased with little or no change in MBD values (Fig. 6*B* – *D*). However, at all ATP concentrations tested, P_o values of S1159F- and S1159P-CFTR were greatly reduced compared to those of wild-type CFTR (Fig. 6*B*). By fitting Michaelis–Menten functions to mean data (Fig. 6*B*), we calculated values of K_D (the ATP concentration required for half-maximal activity, which describes the apparent affinity of CFTR for ATP) and $P_{o(max)}$ (the maximum P_o). For wild-type CFTR, K_D = 0.35 mM and $P_{o(max)}$ = 0.47 (r^2 = 0.97), for S1159F-CFTR, K_D = 0.48 mM and $P_{o(max)}$ = 0.08 (r^2 = 0.93) and for S1159P-CFTR, K_D = 1.42 mM and $P_{o(max)}$ = 0.27 (r^2 = 0.96). These data suggest that both S1159-*CFTR* variants greatly decrease the efficacy with which ATP gates the CFTR Cl^- channel with S1159P-CFTR also reducing the apparent affinity of ATP for CFTR.

Thus, S1159F and S1159P form PKA-activated, ATP-gated CFTR Cl^- channels. They modestly reduce current flow through open channels, but severely decrease P_o by markedly

attenuating the frequency and duration of channel openings. These data indicate that both *CFTR* variants cause class III (regulation) and class IV (conduction) defects (Welsh & Smith, 1993). However, channel activity of S1159F- and S1159P-CFTR was sustained in excised inside-out membrane patches at 37 °C in the presence of PKA and ATP in the intracellular solution ($n \geq 60$; H Li, M Rodrat and DN Sheppard; data not shown). We therefore conclude that S1159-*CFTR* variants do not disrupt the plasma membrane stability of CFTR (Haardt *et al*., 1999).

S1159F- and S1159P-*CFTR* have distinct responses to ivacaftor

Like its effect on G551D-CFTR, ivacaftor robustly potentiated S1159F- and S1159P-CFTR when heterologously expressed in the immortalized human CF bronchial epithelial cell line CFBE41o$^-$ and studied with the Ussing chamber technique (Han *et al*., 2018). To understand better the action of ivacaftor on S1159-*CFTR* variants, we acutely added ivacaftor [10 – 1000 nM, where 500 and 1000 nM are supersaturated concentrations (Csanády & Töröcsik, 2019)] to the intracellular solution bathing excised inside-out membrane patches in the continuous presence of ATP (1 mM) and PKA (75 nM) and studied single-channel behaviour.

Figure 7*A* shows representative recordings of S1159F- and S1159P-CFTR in the absence and presence of ivacaftor (50 and 500 nM) and Figure 7*B* summary P_o-ivacaftor concentration relationships. As controls, Figure 8*A* and Wang *et al*. (2018) show representative single-channel recordings of wild-type and F508del-CFTR in the absence and presence of different concentrations of ivacaftor. By increasing the frequency of channel openings, but not their duration, ivacaftor (10 – 100 nM) doubled the P_o of both S1159-CFTR variants (Fig. 7*A* and *B*). However, the drug did not restore wild-type levels of channel activity (as measured by P_o) to these *CFTR* variants (Figs. 3*E* and 7*A* and *B*). Higher (supersaturated) concentrations of ivacaftor did not increase further the P_o of either S1159F- or S1159P-CFTR (Fig. 7B).

In three membrane patches with single active S1159F-CFTR Cl$^-$ channels, we investigated the effects of ivacaftor on the variant's gating kinetics. In the presence of ivacaftor (50 nM), the open and closed time histograms of S1159F-CFTR remained best fitted with one- and two-component exponential functions described by the same open (τ_{O2}) and closed (τ_{C1}, τ_{C3}) time constants (Fig. 9 and Table 3). Of note, ivacaftor (50 nM) decreased the

slow closed time constant (τ_{C3}) of S1159F-CFTR by 83% to approach that of wild-type CFTR (Figs. 5 and 9 and Tables 2 and 3). However, the drug was without effect on either the open time constant (τ_{O2}) or the fast closed time constant (τ_{C1}) of S1159F-CFTR, which remained greatly reduced and slightly prolonged, respectively, compared with those of wild-type CFTR (Figs. 5 and 9 and Tables 2 and 3).

In contrast to its effects on wild-type CFTR [Fig. 8*A* and Wang *et al*. (2018)], ivacaftor steadily reduced the *i* of S1159F- and S1159P-CFTR at –50 mV (Fig. 7*C*). Figure 7*C* demonstrates that as the ivacaftor concentration increased, the reduction of *i* at –50 mV was modest for S1159P-CFTR, but marked for S1159F-CFTR, such that at the supersaturated ivacaftor concentration of 500 nM, the *i* of S1159F-CFTR was 36% reduced. To understand better this effect of ivacaftor, we constructed single-channel *i-V* relationships at negative voltages for the S1159-*CFTR* variants in the absence and presence of ivacaftor (50 and 500 nM) (Fig. 7*D* and *E*). Ivacaftor (500 nM) caused a slight reduction of the single-channel conductance of S1159P-CFTR, but a substantial decrease for S1159F-CFTR [S1159F-CFTR: control, 8.63 ± 0.55 pS; ivacaftor (500 nM), 4.85 ± 1.06 pS; n = 3; S1159P-CFTR: control = 8.25 ± 1.26 pS; ivacaftor (500 nM), 7.57 ± 1.38 pS; n = 3 – 4].

Ivacaftor inhibition of current flow through S1159F-CFTR is voltage independent

Previous work has identified two mechanisms of CFTR inhibition by small molecules: open-channel blockade and allosteric inhibition (Li & Sheppard, 2009). Open-channel blockers physically occlude the CFTR pore leading to rectification of the *i-V* relationship, whereas allosteric inhibitors act remotely to abrogate current flow through the channel at all voltages tested. To understand better how ivacaftor inhibits S1159F-CFTR, we bathed excised membrane patches in symmetrical Cl^--rich solutions and recorded the single-channel activity of S1159F-CFTR from –60 mV to +60 mV in 20 mV increments in the absence and presence of ivacaftor (100 and 1000 nM) in the intracellular solution, which contained ATP (1 mM) and PKA (75 nM).

Figure 8 shows representative recordings and corresponding current amplitude histograms at ±50 mV of wild-type and S1159F-CFTR Cl^- channels in the absence and presence of ivacaftor (100 nM) and the supersaturated ivacaftor concentration of 1000 nM when bathed in symmetrical Cl^--rich solutions. For wild-type, ivacaftor enhanced greatly the frequency and duration of channel openings at both voltages, without reducing current flow

through the channel (Fig. 8*A*). By contrast, the potentiation of S1159F-CFTR channel gating at both voltages was less marked, while its *i* was reduced (Fig. 8*B*). These different effects of ivacaftor on wild-type and S1159F-CFTR are emphasized by the distinct changes in the single-channel current amplitude histograms elicited by increasing drug concentrations (Fig. 8).

Figure 10 shows summary single-channel P_o-*V* and *i*-*V* relationships for wild-type and S1159F-CFTR. For wild-type CFTR, ivacaftor potentiation of P_o was concentration-dependent, but voltage-independent, while both its *i*-*V* relationship and single-channel conductance were unaffected by increasing concentrations of the drug (Fig. 10*A* – *C*). Although ivacaftor potentiation of the P_o of S1159F-CFTR was voltage-independent, P_o values were maximal at ivacaftor (100 nM) and not further increased at the supersaturated ivacaftor concentration of 1000 nM (Fig. 10*D*). However, ivacaftor (1000 nM) caused a voltage-independent inhibition of the *i*-*V* relationship of S1159F-CFTR, which reduced the single-channel conductance of S1159F-CFTR 2-fold (Fig. 10*E* and *F*). Thus, ivacaftor potentiation of S1159F-CFTR is reduced by allosteric channel inhibition.

DISCUSSION

This study investigated the single-channel behaviour and response to ivacaftor of two rare *CFTR* variants, S1159F and S1159P, which affect the same pore-lining residue in M12. Both *CFTR* variants modestly decreased single-channel conductance, but severely inhibited channel gating. Nanomolar concentrations of ivacaftor potentiated both *CFTR* variants without restoring to them wild-type levels of channel activity, while higher (supersaturated) concentrations decreased the single-channel conductance of S1159F-CFTR.

Many *CFTR* variants, quite likely the majority, cause CFTR dysfunction by several mechanisms. This is highlighted by F508del, which causes a temperature-sensitive folding defect that all but abolishes the biosynthesis of CFTR protein, severely diminishes its plasma membrane stability and gravely disrupts channel gating (Cheng *et al*., 1990; Dalemans *et al*., 1991; Denning *et al*., 1992; Lukacs *et al*., 1993), leading to its categorization as a class II-III-VI *CFTR* variant using the combinatorial classification system for *CFTR* variants (Veit *et al*., 2016). The present results and other data (Han *et al*., 2018; McCarthy *et al*., 2018) reveal that S1159F and S1159P cause conduction and gating defects that diminish CFTR function and suggest that they likely interfere with the biosynthesis of CFTR protein, without affecting its

plasma membrane stability. Two lines of evidence suggest that the S1159-*CFTR* variants reduce the plasma membrane expression of CFTR protein. First, CFTR correctors enhanced the magnitude of CFTR-mediated Cl^- currents generated by immortalized CFBE41o$^-$ and Fischer rat thyroid (FRT) cells heterologously expressing S1159-*CFTR* variants and nasal epithelia from a person with CF with the genotype F508del/S1159P (Han *et al*., 2018; Bihler *et al*., 2023; McCarthy *et al*., 2018). Second, low temperature incubation for ≥ 7 days was required to optimise the plasma membrane expression of S1159-*CFTR* variants for single-channel studies (present study). Consistent with these data, S1159F and S1159P were two of the 177 *CFTR* variants approved for elexacaftor-tezacaftor-ivacaftor combination therapy when the FDA expanded the drug's label (https://www.accessdata.fda.gov/drugsatfda_docs/label/2021/212273s008lbl.pdf). Thus, the molecular basis of CFTR dysfunction caused by the S1159-*CFTR* variants is class II, III and IV defects (Welsh & Smith, 1993), leading to their classification as class II-III *CFTR* variants using the combinatorial classification system (Veit *et al*., 2016).

When compared with other *CFTR* variants in the MSDs that disrupt Cl^- flow through the CFTR channel (e.g. Sheppard *et al*., 1993; Tabcharani *et al*., 1993; Sheppard *et al*., 1996; Gong & Linsdell, 2004), the impact of S1159-*CFTR* variants was reduced. A potential explanation for the diminished severity of these variants on the single-channel conductance of CFTR is the location of S1159 within the CFTR pore. S1159 lies in the deep intracellular vestibule at a level close to the lateral tunnel beneath M4 and M6 through which anions enter the CFTR pore on the intracellular side (Li *et al*., 2018; Zhang *et al*., 2018; Hoffmann *et al*., 2018). At this level, the intracellular vestibule is relatively wide compared to the pore constriction located towards the extracellular side of the plasma membrane (Liu *et al*., 2017; Zhang *et al*., 2018) and other *CFTR* variants in this region have little impact on current flow through the channel (e.g. Seibert *et al*., 1996). Instead, the reduced single-channel conductances of the S1159-*CFTR* variants might reflect their disruption of the hydrogen bond between S1159 and D979 (M9) (Fig. 1). Moreover, the bulky phenylalanine of S1159F clashes with residues in M9, requiring the two transmembrane segments to be further apart in this region, while the proline of S1159P, a known helix breaker (Brandl & Deber, 1986), likely destabilises M12. In support of these ideas, the open-channel pore of CFTR is stabilized by salt-bridges formed between residues in adjacent transmembrane segments [e.g. R347 (M6)-D924 (M8) and R352 (M6)-D993 (M9); Cotten & Welsh, 1999; Cui *et al*., 2008; Zhang *et al*., 2018].

By reducing the frequency and duration of channel openings both S1159-*CFTR* variants severely disrupted the ATP-dependence of CFTR channel gating. These actions of S1159-*CFTR* variants are reminiscent of the *CFTR* gating variants G551D and G1349D (Li *et al*., 1996; Cai *et al*., 2006; Bompadre *et al*., 2007). G551D and G1349D affect key residue in the ABC signature motifs that line the ATP-binding sites located at the NBD1:NBD2 dimer interface [G551D: ATP-binding site 2 (hydrolytic); G1349D: ATP-binding site 1 (non-hydrolytic)] (Aleksandrov *et al*., 2002; Lewis *et al*., 2004; Liu *et al*., 2017; Zhang *et al*., 2018). G551D-CFTR obstructs conformational changes subsequent to ATP binding leading to the loss of ATP-dependent channel gating, whereas G1349D greatly reduces the rate of channel opening and accelerates the rate of channel closure (Cai *et al*., 2006; Bompadre *et al*., 2007). The location of S1159 at the intracellular end of M12, distant from the ATP-binding sites, suggests that S1159F- and S1159P-CFTR act allosterically to perturb channel gating. Consistent with this idea, Kogan *et al*. (2001) demonstrated that obstruction of the CFTR pore either by the open-channel blocker diphenylamine-2-carboxylate or mutagenesis inhibited the ATPase activity of CFTR. Moreover, by combining single-molecule fluorescence resonance energy transfer measurements with single-channel recording with planar lipid bilayers, Levring *et al*. (2023) revealed that c.2780T>C (p.Leu927Pro; legacy: L927P), a *CFTR* variant located in M8 near the transmembrane gating hinge, prevents formation of a tight NBD1:NBD2 dimer and subsequent allosteric coupling, leading to channel opening. Based on these lines of evidence, we posit that the S1159-*CFTR* variants disrupt channel gating by acting allosterically either to inhibit NBD1:NBD2 dimer formation or interfere with coupling between the ATP-binding sites and the transmembrane gating hinge in M8.

Ivacaftor potentiated S1159F- and S1159P-CFTR channel gating leading to a doubling of P_o at nanomolar concentrations. However, the drug's efficacy was conspicuously reduced when compared with its action on the S1159-*CFTR* variants heterologously expressed in the immortalized human CF bronchial epithelial cell line CFBE41o$^-$ (Han *et al*., 2018). Previous work suggests several possible explanations for this difference. First, in epithelia, CFTR activity is modulated by ion channels, transporters and interacting proteins that establish and/or modify the electrochemical gradient for transmembrane anion flow, whereas in cell-free membrane patches, CFTR function is studied directly. Second, CFTR phosphorylation might differ between intact cells and excised inside-out membrane patches, affecting the action of ivacaftor (Cui *et al*., 2019). Under the experimental conditions used, CFTR was

continuously phosphorylated by the constant presence of PKA and ATP, whereas *in vivo* the cellular concentrations of nucleotides determine that the balance of protein kinase and phosphatase activity controls CFTR function (Anderson *et al*., 1991; Anderson & Welsh, 1992; Traut, 1994; Frizzell & Hanrahan, 2012). Third, the cells used for heterologous expression of CFTR [Han *et al*. (2018): CFBE41o$^-$ cells; present study: CHO cells] might influence CFTR function in different ways. Consistent with this idea, Tomati *et al*. (2023) found that elexacaftor-tezacaftor-ivacaftor co-potentiated the *CFTR* variant c.3731G>A (p.Gly1244Glu; legacy: G1244E) when heterologously expressed in CFBE41o$^-$ and FRT cells, but enhanced the plasma membrane expression of CFTR protein in nasal epithelial cells endogenously expressing this *CFTR* variant. Fourth, evidence for cooperativity in CFTR channel gating (Krouse & Wine, 2001) argues that S1159-*CFTR* variants would exhibit greater activity heterologously expressed in polarized CFBE41o$^-$ epithelia where channel density is higher than in excised membrane patches selected for low numbers of active channels. Finally, other factors arising from differences in experimental conditions, most notably the different concentrations of ivacaftor studied [Han *et al*. (2018): 10 μM; present study: 0.01 – 1 μM] might explain the divergent results. Although unlikely to explain the different results obtained by Han *et al*. (2018) and the present study, inflammatory mediators have recently been identified as important regulators of CFTR modulator efficacy that act non-cell autonomously (Gentzsch *et al*., 2021; Rehman *et al*., 2021).

Once the R domain is phosphorylated by PKA, ivacaftor potentiates both ATP-dependent and ATP-independent channel gating by CFTR (Eckford *et al*., 2012; Jih & Hwang, 2013). To prevent irreversible loss of channel activity (Yeh *et al*., 2021), we did not investigate whether ivacaftor potentiates ATP-independent channel gating by the S1159-*CFTR* variants. Ivacaftor potentiation of ATP-dependent channel gating by the S1159-*CFTR* variants differed from the drug's actions on F508del-CFTR in two important respects. First, the different effects of ivacaftor on the pattern of channel gating. Ivacaftor enhanced the frequency of S1159F- and S1159P-CFTR channel openings without prolonging their duration. By contrast, it increased both the frequency and duration of F508del-CFTR channel openings (Van Goor *et al*., 2009; Wang *et al*., 2014). Evidence from biochemical, structural and functional studies (Cholon et al., 2014; Meng *et al*., 2017; Byrnes *et al*., 2018; Wang *et al*., 2018) argue that ivacaftor promotes channel opening by destabilizing a closed channel conformation. Consistent with this idea, the ivacaftor-binding site involves the unstructured region of M8, which gates the channel (Liu *et al*., 2017; Zhang *et al*., 2018; Liu *et al*., 2019;

Yeh *et al*., 2019). An explanation for the prolongation of channel openings by ivacaftor is provided by the energetic coupling model of CFTR channel gating (Jih *et al*., 2012), which revealed that the drug uncouples the gating and catalytic cycles of CFTR (Jih & Hwang, 2013). Alternatively, it might impede channel closure by stabilizing a pre-hydrolytic open state (Langron *et al*., 2018) or bind simultaneously to two independent drug-binding sites with equivalent affinities (Csanády & Töröcsik, 2019). The unstable short-lived open-state of the S1159-*CFTR* variants might explain the failure of ivacaftor to prolong the channel openings of these *CFTR* variants.

The second aspect of ivacaftor potentiation of the S1159-*CFTR* variants which differed from F508del-CFTR was the amount of rescued CFTR function. Ivacaftor doubled the P_o of S1159F- and S1159P-CFTR without restoring to them the P_o of wild-type CFTR. This result contrasts with the drug's action on F508del and other *CFTR* variants including, c.1646G>A (p.Ser549Asn; legacy: S549N), c.1682C>A (p.Ala561Glu; legacy: A561E) and G1244E, where ivacaftor enhanced P_o markedly (Van Goor et al., 2009, Yu et al., 2012, Wang et al., 2014). However, the present data concur with the effects of ivacaftor on G551D, where despite a large enhancement of P_o, wild-type levels were not achieved (Van Goor *et al*., 2009; Yu *et al*., 2012; Wang *et al*., 2014; Liu *et al*., 2022). One potential strategy to restore greater function to the S1159-*CFTR* variants is co-potentiation, the use of two or more potentiators that act at different sites on CFTR to additively enhance channel gating (Phuan *et al*., 2018). To date, co-potentiation has been tested on a limited number of *CFTR* variants with mixed results: some variants (e.g. G551D and G1244E) were amenable to co-potentiation, but others (e.g. F508del and A561E) were not (Phuan *et al*., 2019; Veit *et al*., 2020; Liu *et al*., 2022). Based on values of fractional plasma membrane activity (an indirect measure of P_o relative to that of wild-type CFTR), Veit *et al*. (2020) concluded that *CFTR* gating variants with fractional plasma membrane activity lower than wild-type were receptive to co-potentiation, whereas those with activity equivalent to wild-type were unresponsive. Interestingly, by combining ivacaftor with the high-affinity ATP analogue N^6-(2-phenylethyl)-2'-deoxy-ATP and substituting NO_3^- for Cl^- as the permeant anion, Yu *et al*. (2016) achieved almost complete reversal of the gating defect for the *CFTR* variant c.350G>A (p.Arg117His; legacy: R117H). These data suggest that co-potentiation should augment the restoration of channel function to S1159-*CFTR* variants. Future studies should test this idea.

Previous studies demonstrate that micromolar concentrations of ivacaftor attenuate the plasma membrane expression and function of some *CFTR* variants (Cholon *et al*., 2014; Veit *et al*., 2014; Wang *et al*., 2014; Avramescu *et al*., 2017). For example, micromolar concentrations of ivacaftor inhibit F508del-CFTR both by destabilizing its structure (Cholon *et al*., 2014; Veit *et al*., 2014) and disrupting the integrity of the lipid bilayer (Chin *et al*., 2018). The physicochemical properties of ivacaftor provide an explanation for the deleterious actions of micromolar concentrations of ivacaftor on CFTR (Csanády & Töröcsik, 2019). The aqueous solubility of ivacaftor at 37 °C is 138 nM, its octanol/water distribution coefficient is ~60000 (i.e. when $[\text{ivacaftor}]_{\text{aqueous}}$ = 1 μM, $[\text{ivacaftor}]_{\text{membrane}}$ = 60 mM) and at physiological pH, ivacaftor is uncharged (Csanády & Töröcsik, 2019). Importantly, using thermodynamic arguments, the authors demonstrated that the concentration of free drug in solution, which is in equilibrium with that in cellular membranes cannot exceed the solubility limit of ivacaftor. Thus, under the experimental conditions employed in the present study, solutions containing ivacaftor (0.5 and 1 μM) are supersaturated, leading to supersaturation of excised membrane patches, which are in equilibrium with the ivacaftor solutions. Although precipitation of ivacaftor from supersaturated solutions is slow due to its low concentration, the octanol/water distribution coefficient of ivacaftor results in the rapid accumulation of excessive quantities of ivacaftor in excised membrane patches, predisposing to the formation of crystalline precipitates, which perturb the physicochemical properties of the membrane (Csanády & Töröcsik, 2019).

In the case of S1159F-CFTR and to a lesser extent S1159P-CFTR, membrane accumulation of ivacaftor likely accentuates allosteric inhibition of current flow through open channels. The location of the ivacaftor-binding site at a pivotal position within the MSDs for CFTR gating and permeation (Liu *et al*., 2019; Yeh *et al*., 2019) (Fig. 1) provides one explanation for how the interaction of ivacaftor with S1159F might obstruct Cl^- flow through the channel by an allosteric mechanism. Alternatively, ivacaftor might inhibit S1159F-CFTR by interacting with a different binding site. Consistent with this idea, using photoactivatable ivacaftor probes and HEK-293 cells heterologously expressing wild-type CFTR, Laselva *et al*. (2021) localised an additional binding site for ivacaftor on intracellular loop 4 at the interface between the NBDs and MSDs. The interaction of ivacaftor with this second site might lead to allosteric inhibition of the S1159F-CFTR Cl^- channel. Future studies of ivacaftor's action on *CFTR* variants should be mindful to avoid supersaturating

concentrations of the drug and alert to the possibility that it might inhibit the channel under some experimental conditions.

In conclusion, the pore-lining residue S1159 in M12 is the site of two rare *CFTR* variants with similar molecular mechanisms of CFTR dysfunction but distinct responses to ivacaftor. S1159F and S1159P principally diminish CFTR function by gravely impeding ATP-dependent channel gating with S1159F causing the greater adverse effect consistent with its more severe clinical phenotype (Table 1) (https://cftr2.org/). Together with their impacts on the trafficking of CFTR protein to the plasma membrane and current flow through open channels, the combinatorial classification of the S1159-*CFTR* variants is class II-III (Veit *et al*., 2016), a theratype requiring a combination of CFTR correctors and potentiators to restore channel function. However, the failure of physiologically relevant ivacaftor concentrations to confer the P_o of wild-type CFTR on S1159F- and S1159P-CFTR argues that multiple correctors and potentiators will likely be required for optimal treatment of people with CF and S1159-*CFTR* variants using CFTR-targeted therapeutics. Thus, this study illustrates the importance of detailed investigations of CFTR function and pharmacology to understand the causes of phenotypic differences between individual *CFTR* variants.

REFERENCES

Aleksandrov, L., Aleksandrov, A. A., Chang, X.-B., & Riordan, J. R. (2002). The first nucleotide binding domain of cystic fibrosis transmembrane conductance regulator is a site of stable nucleotide interaction, whereas the second is a site of rapid turnover. *The Journal of Biological Chemistry* **277**, 15419-15425.

Anderson, M. P., & Welsh, M. J. (1992). Regulation by ATP and ADP of CFTR chloride channels that contain mutant nucleotide-binding domains. *Science* **257**, 1701-1704.

Anderson, M. P., Berger, H. A., Rich, D. P., Gregory, R. J., Smith, A. E., & Welsh, M. J. (1991). Nucleoside triphosphates are required to open the CFTR chloride channel. *Cell* **67**, 775-784.

Avramescu, R. G., Kai, Y., Xu, H., Bidaud-Meynard, A., Schnúr, A., Frenkiel, S., Matouk, E., Veit, G., & Lukacs, G. L. (2017). Mutation-specific downregulation of CFTR2 variants by gating potentiators. *Human Molecular Genetics* **26**, 4873-4885.

Bihler, H., Sivachenko, A., Millen, L., Bhatt, P., Thakerar Patel, A., Chin, J., Bailey, V., Musisi, I., LaPan, A., Allaire, N. E., Conte, J., Simon, N. R., Magaret, A. S., Raraigh, K. S., Cutting, G. R., Skach, W. R., Bridges, R. J., Thomas, P. J., & Mense, M. (2023). *In vitro* modulator responsiveness of 655 *CFTR* variants found in people with CF. *bioRxiv* DOI: 10.1101/2023.07.07.548159.

Bompadre, S. G., Sohma, Y., Li, M., & Hwang, T.-C. (2007). G551D and G1349D, two CF-associated mutations in the signature sequences of CFTR, exhibit distinct gating defects. *The Journal of General Physiology* **129**, 285-298.

Bose, S. J., Bijvelds, M. J. C., Wang, Y., Liu, J., Cai, Z., Bot, A. G. M., de Jonge, H. R., & Sheppard, D. N. (2019). Differential thermostability and response to cystic fibrosis transmembrane conductance regulator potentiators of human and mouse F508del-CFTR. *American Journal of Physiology. Lung Cellular and Molecular Physiology* **317**, L71-L86.

Brandl, C. J., & Deber, C. M. (1986). Hypothesis about the function of membrane-buried proline residues in transport proteins. *Proceedings of the National Academy of Sciences of the USA* **83**, 917-921.

Byrnes, L. J., Xu, Y., Qiu, X., Hall, J. D., & West, G. M. (2018). Sites associated with Kalydeco binding on human cystic fibrosis transmembrane conductance regulator revealed by hydrogen/deuterium exchange. *Scientific Reports* **8**, 4664.

Cai, Z., Palmai-Pallag, T., Khuituan, P., Mutolo, M. J., Boinot, C., Liu, B., Scott-Ward, T. S., Callebaut, I., Harris, A., & Sheppard, D. N. (2015). Impact of the F508del mutation on ovine CFTR, a Cl^- channel with enhanced conductance and ATP-dependent gating. *The Journal of Physiology* **593**, 2427-2446.

Cai, Z., Scott-Ward, T. S., & Sheppard, D. N. (2003). Voltage-dependent gating of the cystic fibrosis transmembrane conductance regulator Cl^- channel. *The Journal of General Physiology* **122**, 605-620.

Cai, Z., Taddei, A., & Sheppard, D. N. (2006). Differential sensitivity of the cystic fibrosis (CF)-associated mutants G551D and G1349D to potentiators of the cystic fibrosis transmembrane conductance regulator (CFTR) Cl^- channel. *The Journal of Biological Chemistry* **281**, 1970-1977.

Chen, J.-H., Cai, Z., & Sheppard, D. N. (2009). Direct sensing of intracellular pH by the cystic fibrosis transmembrane conductance regulator (CFTR) Cl^- channel. *The Journal of Biological Chemistry* **284**, 35495-35506.

Cheng, S. H., Gregory, R. J., Marshall, J., Paul, S., Souza, D. W., White, G. A., O'Riordan, C. R., & Smith, A. E. (1990). Defective intracellular transport and processing of CFTR is the molecular basis of most cystic fibrosis. *Cell* **63**, 827-834.

Chin, S., Hung, M., Won, A., Wu, Y.-S., Ahmadi, S., Yang, D., Elmallah, S., Toutah, K., Hamilton, C. M., Young, R. N., Viirre, R. D., Yip, C. M., & Bear, C. E. (2018). Lipophilicity of the cystic fibrosis drug, ivacaftor (VX-770), and its destabilizing effect on the major CF-causing mutation: F508del. *Molecular Pharmacology* **94**, 917-925.

Cholon, D. M., Quinney, N. L., Fulcher, M. L., Esther, C. R., Das, J., Dokholyan, N. V., Randell, S. H., Boucher, R. C., & Gentzsch, M. (2014). Potentiator ivacaftor abrogates pharmacological correction of ΔF508 CFTR in cystic fibrosis. *Science Translational Medicine* **6**, 246ra96.

Cotton, J. F., & Welsh, M. J. (1999). Cystic fibrosis-associated mutations at arginine 347 alter the pore architecture of CFTR. *The Journal of Biological Chemistry* **274**, 5429-5435.

Csanády, L., & Töröcsik, B. (2019). Cystic fibrosis drug ivacaftor stimulates CFTR channels at picomolar concentrations. *eLife* **8**, e46450.

Cui, G., Stauffer, B. B., Imhoff, B. R., Rab, A., Hong, J. S., Sorscher, E. J., & McCarty, N. A. (2019). VX-770-mediated potentiation of numerous human CFTR disease mutants is influenced by phosphorylation level. *Scientific Reports* **9**, 13460.

Cui, G., Zhang, Z.-R., O'Brien, A. R. W., Song, B., & McCarty, N. A. (2008). Mutations at arginine 352 alter the pore architecture of CFTR. *The Journal of Membrane Biology* **222**, 91-106.

Cutting, G. R. (2015). Cystic fibrosis genetics: from molecular understanding to clinical application. *Nature Reviews. Genetics* **16**, 45-56.

Dalemans, W., Barbry, P., Champigny, G., Jallat, S., Dott, K., Dreyer, D., Crystal, R. G., Pavirani, A., Lecocq, J.-P., & Lazdunski, M. (1991). Altered chloride ion channel kinetics associated with the ΔF508 cystic fibrosis mutation. *Nature* **354**, 526-528.

Denning, G. M., Anderson, M. P., Amara, J. F., Marshall, J., Smith, A. E., & Welsh, M. J. (1992). Processing of mutant cystic fibrosis transmembrane conductance regulator is temperature-sensitive. *Nature* **358**, 761-764.

Eckford, P. D. W., Li, C., Ramjeesingh, M., & Bear, C. E. (2012). Cystic fibrosis transmembrane conductance regulator (CFTR) potentiator VX-770 (ivacaftor) opens the

defective channel gate of mutant CFTR in a phosphorylation-dependent but ATP-independent manner. *The Journal of Biolgical Chemistry* **287**, 36639-36649.

Farrell, P. M., White, T. B., Ren, C. L., Hempstead, S. E., Accurso, F., Derichs, N., Howenstine, M., McColley, S. A., Rock, M., Rosenfeld, M., Sermet-Gaudelus, I., Southern, K. W., Marshall, B. C., & Sosnay, P. R. (2017). Diagnosis of cystic fibrosis: consensus guidelines from the Cystic Fibrosis Foundation. *The Journal of Pediatrics* **181**, S4-S15.e1.

Frizzell, R. A., & Hanrahan, J. W. (2012). Physiology of epithelial chloride and fluid secretion. *Cold Spring Harbor Perspectives in Medicine* **2**, a009563.

Gentzsch, M., Cholon, D. M., Quinney, N. L., Martino, M. E. B., Minges, J. T., Boyles, S. E., Guhr Lee, T. N., Esther, C. R., & Ribeiro, C. M. P. (2021). Airway epithelial inflammation *in vitro* augments the rescue of mutant CFTR by current CFTR modulator therapies. *Frontier in Pharmacology* **12**, 628722.

Gong, X., & Linsdell, P. (2004). Maximization of the rate of chloride conduction in the CFTR channel pore by ion–ion interactions. *Archives of Biochemistry and Biophysics* **426**, 78-82.

Haardt, M., Benharouga, M., Lechardeur, D., Kartner, N., & Lukacs, G. L. (1999). C-terminal truncations destabilize the cystic fibrosis transmembrane conductance regulator without impairing its biogenesis: a novel class of mutation. *The Journal of Biological Chemistry* **274**, 21873-21877.

Han, S. T., Rab, A., Pellicore, M. J., Davis, E. F., McCague, A. F., Evans, T. A., Joynt, A. T., Lu, Z., Cai, Z., Raraigh, K. S., Hong, J. S., Sheppard, D. N., Sorscher, E. J., & Cutting, G. R. (2018). Residual function of cystic fibrosis mutants predicts response to small molecule CFTR modulators. *JCI Insight* **3**, e121159.

Heijerman, H. G. M., McKone, E. F., Downey, D. G., Van Braeckel, E., Rowe, S. M., Tullis, E., Mall, M. A., Welter, J. J., Ramsey, B. W., McKee, C. M., Marigowda, G., Moskowitz, S. M., Waltz, D., Sosnay, P. R., Simard, C., Ahluwalia, N., Xuan, F., Zhang, Y., Taylor-Cousar, J. L., & McCoy, K. S.; VX17-445-103 Trial Group. (2019). Efficacy and safety of the elexacaftor plus tezacaftor plus ivacaftor combination regimen in people with cystic fibrosis

homozygous for the F508del mutation: a double-blind, randomised, phase 3 trial. *Lancet* **394**, 1940-1948.

Hoffmann, B., Elbahnsi, A., Lehn, P., Décout, J.-L., Pietrucci, F., Mornon, J.-P., & Callebaut, I. (2018). Combining theoretical and experimental data to decipher CFTR 3D structures and functions. *Cellular and Molecular Life Sciences* **75**, 3829-3855.

Hwang, T.-C., Yeh, J.-T., Zhang, J., Yu, Y.-C., Yeh, H.-I., & Destefano, S. (2018). Structural mechanisms of CFTR function and dysfunction. *The Journal of General Physiology* **150**, 539-570.

Jih, K.-Y., & Hwang, T.-C. (2013). Vx-770 potentiates CFTR function by promoting decoupling between the gating cycle and ATP hydrolysis cycle. *Proceedings of the National Academy of Sciences of the USA* **110**, 4404-4409.

Jih, K.-Y., Sohma, Y., & Hwang, T.-C. (2012). Nonintegral stoichiometry in CFTR gating revealed by a pore-lining mutation. *The Journal of General Physiology* **140**, 347-359.

Knowles, M. R., & Durie, P. R. (2002). What is cystic fibrosis? *The New England Journal of Medicine* **347**, 439-442.

Kogan, I., Ramjeesingh, M., Huan, L.-J., Wang, Y., & Bear, C. E. (2001). Perturbation of the pore of the cystic fibrosis transmembrane conductance regulator (CFTR) inhibits its ATPase activity. *The Journal of Biological Chemistry* **276**, 11575-11581.

Krouse, M. E., & Wine, J. J. (2001). Evidence that CFTR channels can regulate the open duration of other CFTR channels: cooperativity. *The Journal of Membrane Biology* **182**, 223-232.

Langron, E., Prins, S., & Vergani, P. (2018). Potentiation of the cystic fibrosis transmembrane conductance regulator by VX-770 involves stabilization of the pre-hydrolytic, O_1 state. *British Journal of Pharmacology* **175**, 3990-4002.

Lansdell, K. A., Delaney, S. J., Lunn, D. P., Thomson, S. A., Sheppard, D. N., & Wainwright, B. J. (1998). Comparison of the gating behaviour of human and murine cystic fibrosis transmembrane conductance regulator Cl^- channels expressed in mammalian cells. *The Journal of Physiology* **508**, 379-392.

Laselva, O., Qureshi, Z., Zeng, Z.-W., Petrotchenko, E. V., Ramjeesingh, M., Hamilton, C. M., Huan, L.-J., Borchers, C. H., Pomès, R., Young, R., & Bear, C. E. (2021). Identification of binding sites for ivacaftor on the cystic fibrosis transmembrane conductance regulator. *iScience* **24**, 102542.

Levring, J., Terry, D. S., Kilic, Z., Fitzgerald, G., Blanchard, S. C., & Chen, J. (2023). CFTR function, pathology and pharmacology at single-molecule resolution. *Nature* **616**, 606-614.

Lewis, H. A., Buchanan, S. G., Burley, S. K., Conners, K., Dickey, M., Dorwart, M., Fowler, R., Gao, X., Guggino, W. B., Hendrickson, W. A., Hunt, J. F., Kearins, M. C., Lorimer, D., Maloney, P. C., Post, K. W., Rajashankar, K. R., Rutter, M. E., Sauder, J. M., Shriver, S., … Emtage, S. (2004). Structure of nucleotide-binding domain 1 of the cystic fibrosis transmembrane conductance regulator. *The EMBO Journal* **23**, 282-293.

Li, C., Ramjeesingh, M., Wang, W., Garami, E., Hewryk, M., Lee, D., Rommens, J. M., Galley, K., & Bear, C. E. (1996). ATPase activity of the cystic fibrosis transmembrane conductance regulator. *The Journal of Biological Chemistry* **271**, 28463-28468.

Li, H., & Sheppard, D. N. (2009). Therapeutic potential of cystic fibrosis transmembrane conductance regulator (CFTR) inhibitors in polycystic kidney disease. *BioDrugs* **23**, 203-216.

Li, M.-S., Cowley, E. A., El Hiani, Y., & Linsdell, P. (2018). Functional organization of cytoplasmic portals controlling access to the cystic fibrosis transmembrane conductance regulator (CFTR) chloride channel pore. *The Journal of Biological Chemistry* **293**, 5649-5658.

Liu, F., Zhang, Z., Csanády, L., Gadsby, D. C., & Chen, J. (2017). Molecular structure of the human CFTR ion channel. *Cell* **169**, 85-95.e8.

Liu, F., Zhang, Z., Levit, A., Levring, J., Touhara, K. K., Shoichet, B. K., & Chen, J. (2019). Structural identification of a hotspot on CFTR for potentiation. *Science* **364**, 1184-1188.

Liu, J., Berg, A. P., Wang, Y., Jantarajit, W., Sutcliffe, K. J., Stevens, E. B., Cao, L., Pregel, M. J., & Sheppard, D. N. (2022). A small molecule CFTR potentiator restores ATP-dependent channel gating to the cystic fibrosis mutant G551D-CFTR. *British Journal of Pharmacology* **179**, 1319-1337.

Lukacs, G. L., Chang, X.-B., Bear, C., Kartner, N., Mohamed, A., Riordan, J. R., & Grinstein, S. (1993). The ΔF508 mutation decreases the stability of cystic fibrosis transmembrane conductance regulator in the plasma membrane. Determination of functional half-lives on transfected cells. *The Journal of Biological Chemistry* **268**, 21592-21598.

Marshall, J., Fang, S., Ostedgaard, L. S., O'Riordan, C. R., Ferrara, D., Amara, J. F., Hoppe, H. IV, Scheule, R. K., Welsh, M. J., & Smith, A. E. (1994). Stoichiometry of recombinant cystic fibrosis transmembrane conductance regulator in epithelial cells and its functional reconstitution into cells *in vitro*. *The Journal of Biological Chemistry* **269**, 2987-2995.

McCarthy, C., Brewington, J. J., Harkness, B., Clancy, J. P., & Trapnell, B. C. (2018). Personalised CFTR pharmacotherapeutic response testing and therapy of cystic fibrosis. *The European Respiratory Journal* **51**, 1702457.

Meng, X., Wang, Y., Wang, X., Wrennall, J. A., Rimington, T. L., Li, H., Cai, Z., Ford, R. C., & Sheppard, D. N. (2017). Two small molecules restore stability to a subpopulation of the cystic fibrosis transmembrane conductance regulator with the predominant disease-causing mutation. *The Journal of Biological Chemistry* **292**, 3706-3719.

Middleton, P. G., Mall, M. A., Dřevínek, P., Lands, L. C., McKone, E. F., Polineni, D., Ramsey, B. W., Taylor-Cousar, J. L., Tullis, E., Vermeulen, F., Marigowda, G., McKee, C. M., Moskowitz, S. M., Nair, N., Savage, J., Simard, C., Tian, S., Waltz, D., Xuan, F., … Jain, R.; VX17-445-102 Study Group. (2019). Elexacaftor–tezacaftor–ivacaftor for cystic fibrosis with a single Phe508del allele. *The New England Journal of Medicine* **381**, 1809-1819.

Phuan, P.-W., Son, J.-H., Tan, J.-A., Li, C., Musante, I., Zlock, L., Nielson, D. W., Finkbeiner, W. E., Kurth, M. J., Galietta, L. J., Haggie, P. M., & Verkman, A. S. (2018). Combination potentiator ('co-potentiator') therapy for CF caused by CFTR mutants, including N1303K, that are poorly responsive to single potentiators. *Journal of Cystic Fibrosis* **17**, 595-606.

Phuan, P.-W., Tan, J.-A., Rivera., A. A., Zlock, L., Nielson, D. W., Finkbeiner, W. E., Haggie, P. M., & Verkman, A. S. (2019). Nanomolar-potency 'co-potentiator' therapy for cystic fibrosis caused by a defined subset of minimal function CFTR mutants. *Scientific Reports* **9**, 17640.

Ramsey, B. W., Davies, J., McElvaney, N. G., Tullis, E., Bell, S. C., Dřevínek, P., Griese, M., McKone, E. F., Wainwright, C. E., Konstan, M. W., Moss, R., Ratjen, F., Sermet-Gaudelus, I., Rowe, S. M., Dong, Q., Rodriguez, S., Yen, K., Ordoñez, C., & Elborn, J. S.; VX08-770-102 Study Group. (2011). A CFTR potentiator in patients with cystic fibrosis and the *G551D* mutation. *The New England Journal of Medicine* **365**, 1663-1672.

Ratjen, F., Bell, S. C., Rowe, S. M., Goss, C. H., Quittner, A. L., & Bush, A. (2015). Cystic fibrosis. *Nature Reviews. Disease Primers* **1**, 15010.

Rehman, T., Karp, P. H., Tan, P., Goodell, B. J., Pezzulo, A. A., Thurman, A. L., Thornell, I. M., Durfey, S. L., Duffey, M. E., Stoltz, D. A., McKone, E. F., Singh, P. K., & Welsh, M. J. (2021). Inflammatory cytokines TNF-α and IL-17 enhance the efficacy of cystic fibrosis transmembrane conductance regulator modulators. *The Journal of Clinical Investigation* **131**, e150398.

Seibert, F. S., Linsdell, P., Loo, T. W., Hanrahan, J. W., Riordan, J. R., & Clarke, D. M. (1996). Cytoplasmic loop three of cystic fibrosis transmembrane conductance regulator contributes to regulation of chloride channel activity. *The Journal of Biological Chemistry* **271**, 27493-27499.

Sheppard, D. N., Rich, D. P., Ostedgaard, L. S., Gregory, R. J., Smith, A. E., & Welsh, M. J. (1993). Mutations in CFTR associated with mild-disease-form Cl^- channels with altered pore properties. *Nature* **362**, 160-164.

Sheppard, D. N., & Robinson, K. A. (1997). Mechanism of glibenclamide inhibition of cystic fibrosis transmembrane conductance regulator Cl^- channels expressed in a murine cell line. *The Journal of Physiology* **503**, 333-346.

Sheppard, D. N., Travis, S. M., Ishihara, H., & Welsh, M. J. (1996). Contribution of proline residues in the membrane-spanning domains of cystic fibrosis transmembrane conductance regulator to chloride channel function. *The Journal of Biological Chemistry* **271**, 14995-15001.

Tabcharani, J. A., Rommens, J. M., Hou, Y.-X., Chang, X.-B., Tsui, L.-C., Riordan, J. R., & Hanrahan, J. W. (1993). Multi-ion pore behaviour in the CFTR chloride channel. *Nature* **366** 79-82.

Tomati, V., Costa, S., Capurro, V., Pesce, E., Pastorino, C., Lena, M., Sondo, E., Di Duca, M., Cresta, F., Cristadoro, S., Zara, F., Galietta, L. J. V., Bocciardi, R., Castellani, C., Lucanto, M. C., & Pedemonte, N. (2023). Rescue by elexacaftor-tezacaftor-ivacaftor of the G1244E cystic fibrosis mutation's stability and gating defects are dependent on cell background. *Journal of Cystic Fibrosis* **22**, 525-537.

Traut, T. W. (1994). Physiological concentrations of purines and pyrimidines. *Molecular and Cellular Biochemistry* **140**, 1-22.

Van Goor, F., Hadida, S., Grootenhuis, P. D. J., Burton, B., Cao, D., Neuberger, T., Turnbull, A., Singh, A., Joubran, J., Hazlewood, A., Zhou, J., McCartney, J., Arumugam, V., Decker, C., Yang, J., Young, C., Olson, E. R., Wine, J. J., Frizzell, R. A., … Negulescu, P. (2009). Rescue of CF airway epithelial cell function in vitro by a CFTR potentiator, VX-770. *Proceedings of the National Academy of Sciences of the USA* **106**, 18825-18830.

Veit, G., Avramescu, R. G., Chiang, A. N., Houck, S. A., Cai, Z., Peters, K. W., Hong, J. S., Pollard, H. B., Guggino, W. B., Balch, W. E., Skach, W. R., Cutting, G. R., Frizzell, R. A., Sheppard, D. N., Cyr, D. M., Sorscher, E. J., Brodsky, J. L., & Lukacs, G. L. (2016). From CFTR biology toward combinatorial pharmacotherapy: expanded classification of cystic fibrosis mutations. *Molecular Biology of the Cell* **27**, 424-433.

Veit, G., Avramescu, R. G., Perdomo, D., Phuan, P. W., Bagdany, M., Apaja, P. M., Borot, F., Szollosi, D., Wu, Y. S., Finkbeiner, W. E., Hegedus, T., Verkman, A. S., & Lukacs, G. L. (2014). Some gating potentiators, including VX-770, diminish ΔF508-CFTR functional expression. *Science Translational Medicine* **6**, 246ra97.

Veit, G., Da Fonte, D. F., Avramescu, R. G., Premchandar, A., Bagdany, M., Xu, H., Bensinger, D., Stubba, D., Schmidt, B., Matouk, E., & Lukacs, G. L. (2020). Mutation-specific dual potentiators maximize rescue of CFTR gating mutants. *Journal of Cystic Fibrosis* **19**, 236-244.

Venglarik, C. J., Schultz, B. D., Frizzell, R. A., & Bridges, R. J. (1994). ATP alters current fluctuations of cystic fibrosis transmembrane conductance regulator: evidence for a three-state activation mechanism. *The Journal of General Physiology* **104**, 123-146.

Wang, Y., Cai, Z., Gosling, M., & Sheppard, D. N. (2018). Potentiation of the cystic fibrosis transmembrane conductance regulator Cl^- channel by ivacaftor is temperature independent. *American Journal of Physiology. Lung Cellular and Molecular Physiology* **315**, L846-L857.

Wang, Y., Liu, J., Loizidou, A., Bugeja, L. A., Warner, R., Hawley, B. R., Cai, Z., Toye, A. M., Sheppard, D. N., & Li, H. (2014). CFTR potentiators partially restore channel function to A561E-CFTR, a cystic fibrosis mutant with a similar mechanism of dysfunction as F508del-CFTR. *British Journal of Pharmacology* **171**, 4490-4503.

Welsh, M. J., & Smith, A. E. (1993). Molecular mechanisms of CFTR chloride channel dysfunction in cystic fibrosis. *Cell* **73**, 1251-1254.

Yeh, H.-I., Qiu, L., Sohma, Y., Conrath, K., Zou, X., & Hwang, T.-C. (2019). Identifying the molecular target sites for CFTR potentiators GLPG1837 and VX-770. *The Journal of General Physiology* **151**, 912-928.

Yeh, H.-I., Sutcliffe, K. J., Sheppard, D. N., & Hwang, T.-C. (2022) CFTR modulators: from mechanism to targeted therapeutics. *Handbook of Experimental Pharmacology*. Advance online publication. https://doi.org/10.1007/164_2022_597

Yeh, H.-I., Yu, Y.-C., Kuo, P.-L., Tsai, C.-K., Huang, H.-T., & Hwang, T.-C. (2021). Functional stability of CFTR depends on tight binding of ATP at its degenerate ATP-binding site. *The Journal of Physiology* **599**, 4625-4642.

Yu, H., Burton, B., Huang, C.-J., Worley, J., Cao, D., Johnson, J. P., Urrutia, A., Joubran, J., Seepersaud, S., Sussky, K., Hoffman, B. J., & Van Goor, F. (2012). Ivacaftor potentiation of multiple CFTR channels with gating mutations. *Journal of Cystic Fibrosis* **11**, 237-245.

Yu, Y.-C., Sohma, Y., & Hwang, T.-C. (2016). On the mechanism of gating defects caused by the R117H mutation in cystic fibrosis transmembrane conductance regulator. *The Journal of Physiology* **594**, 3227-3244.

Zhang, Z., Liu, F., & Chen, J. (2018). Molecular structure of the ATP-bound, phosphorylated human CFTR. *Proceedings of the National Academy of Sciences of the USA* **115**, 12757-12762.

ADDITIONAL INFORMATION

Data availability statement

Data are available at the University of Bristol data repository, data.bris, at https://doi.org/10.5523/bris.kufnj4dzb73x243mox1v5inha.

Competing interests

The authors have no conflicts of interest to declare.

Author contributions

S1159-CFTR cDNAs were synthesized at Johns Hopkins University and studied using the patch-clamp technique at the University of Bristol. Conception and design of experiments: H.L., G.R.C. and D.N.S.; performed the research: H.L., M.R., and S.T.H.; analysis and interpretation of data: H.L., M.R., M.K.A.-S., D.-F.V., K.S.R., G.R.C. and D.N.S.; drafting the manuscript or revising it critically for important intellectual content: H.L., M.R., M.K.A.-S., D.-F.V., S.T.H., K.S.R., G.R.C. and D.N.S.. All authors have read and approved the final version of this manuscript and agree to be accountable for all aspects of the work in ensuring that questions related to the accuracy or integrity of any part of the work are appropriately investigated and resolved. All persons designated as authors qualify for authorship and all those who qualify for authorship are listed.

Funding

This work was supported by Cystic Fibrosis Foundation Therapeutics [grant no. SHEPPA14XX0] and the Cystic Fibrosis Trust [grant nos. SRC 005 and SRC 021] to D.N.S. and Cystic Fibrosis Foundation [grant no. CUTT13A1] and National Institute of Diabetes and Digestive and Kidney Diseases [grant no. R01 DK44003] to G.R.C.. During part of this work, M.R. was supported by The Royal Golden Jubilee PhD Program, co-funded by the Thailand Research Fund and the UK Newton Fund (grant no. PHD/0105/2557). M.K.A.-S. was the recipient of a scholarship and research funding from the Ministry of Higher Education, Research and Innovation of the Sultanate of Oman.

Acknowledgements

We thank C.R. O'Riordan for CFTR-expressing cells and M.J.C. Bijvelds, C. Govaerts, M.W. van der Kamp, P. Vergani and laboratory colleagues for valuable discussions and assistance.

Author's present address

S.T. Han: New York Genome Center, 101 Avenue of the Americas, New York, NY 10013, USA.

TABLES

Table 1: Clinical characteristics of individuals with S1159 *CFTR* variants and a *CFTR* variant that causes pancreatic insufficiency

	Age (years) at time of data collection	Sweat [Cl^-] (mmol L^{-1})	Age (years) at time of PFTs[a]	$ppFEV_1$ (%)[b]	Pancreatic insufficiency (%)[c]	*Pseudomonas. aeruginosa* (%)[d]
Individuals with S1159F and a *CFTR* variant associated with pancreatic insufficiency (*n* = 20)						
Average	22	90	26	74	67	56
Minimum	2	63	9	28		
Maximum	60	133	59	117		
Individuals with S1159P and a *CFTR* variant associated with pancreatic insufficiency (*n* = 19)						
Average	33	77	37	71	35	62
Minimum	2	11	9	32		
Maximum	83	113	83	102		

Sweat [Cl^-] values diagnostic of CF are: non-CF, < 30 mmol L^{-1}; CFTR residual function, 30 – 59 mmol L^{-1}; CFTR minimal function, > 60 mmol L^{-1} (Farrell *et al*., 2017). Lung function in non-CF individuals is 80 – 120% $ppFEV_1$; < 1% of non-CF individuals are pancreatic insufficient; < 1% of non-CF individuals have lung infections with *Pseudomonas aeruginosa*. *CFTR* variants associated with pancreatic sufficiency are dominant over those associated with pancreatic insufficiency. For further information, see https://cftr2.org/.

[a] pulmonary function tests; [b] percent predicted forced expiratory volume in one second determined using the Global Lung Function Initiative calculator (https://gli-calculator.ersnet.org/); [c] pancreatic insufficiency indicates loss of exocrine pancreatic function; [d] CF respiratory microbial pathogen.

Table 2. Open and closed time constants of S1159-*CFTR* variants

	***CFTR* variant**		
	Wild-type	S1159F	S1159P
τ_{O2} (ms)	33.3 ± 6.0	7.2 ± 0.8	10.6 ± 5.4
τ_{C1} (ms)	2.4 ± 0.4	3.2 ± 0.8	3.8 ± 2.8
τ_{C3} (ms)	187 ± 55	1,149 ± 321	434 ± 147
Area under curve τ_{C1}	0.76 ± 0.08	0.63 ± 0.21	0.64 ± 0.30
Area under curve τ_{C3}	0.24 ± 0.08	0.37 ± 0.21	0.36 ± 0.30
Events per minute	696 ± 257	132 ± 26	389 ± 274
Total time (s)	1,009	1,032	943
n	3	3	3

Time constants (τ_{O2}, slow open time constant; τ_{C1}, fast closed time constant; τ_{C3}, slow closed time constant) were derived from the fitting of one- or two-component exponential functions to open and closed time histograms using the maximum likelihood method as described in the Methods. [Open and slow closed time constants are designated τ_{O2} and τ_{C3}, respectively, for consistency with previous studies, where open-channel blockers induced additional populations of open and closed times fit with fast open time (τ_{O1}) and intermediate closed time (τ_{C2}) constants (Sheppard & Robinson, 1997)]. Area under curve indicates the proportion of the total closed time distribution that corresponds to the different closed time constants. Events per minute represents the total number of transitions between the open and closed states within one minute. The total time analysed for wild-type, S1159F- and S1159P-CFTR is shown and in each patch, approximately 5,000 events were analysed for wild-type CFTR, 800 for S1159F-CFTR and 1,000 for S1159P-CFTR. Values are means ± SD of *n* observations. Measurements were made at 37 °C in the presence of the catalytic subunit of PKA (75 nM) and ATP (1 mM) in the intracellular solution; voltage was –50 mV and there was a large Cl^- concentration gradient across the membrane patch ($[Cl^-]_{int}$, 147 mM; $[Cl^-]_{ext}$, 10 mM).

Table 3. Effects of ivacaftor (50 nM) on the open and closed time constants of S1159F-CFTR

	S1159F	
	Control	Ivacaftor
τ_{O2} (ms)	6.3 ± 1.8	5.7 ± 1.5
τ_{C1} (ms)	4.7 ± 2.4	3.4 ± 1.3
τ_{C3} (ms)	1,970 ± 1,527	338 ± 57
Area under curve τ_{C1}	0.65 ± 0.11	0.69 ± 0.21
Area under curve τ_{C3}	0.35 ± 0.11	0.31 ± 0.21
Events per minute	154 ± 160	512 ± 229
Total time (s)	1,578	1,111
n	3	3

Time constants (τ_{O2}, slow open time constant; τ_{C1}, fast closed time constant; τ_{C3}, slow closed time constant) were derived from the fitting of one- or two-component exponential functions to open and closed time histograms using the maximum likelihood method as described in the Methods. Area under curve indicates the proportion of the total closed time distribution that corresponds to the different closed time constants. Events per minute represents the total number of transitions between the open and closed states within one minute. The total time analysed is shown and in each patch, approximately 1,000 and 3,000 events were analysed in the absence and presence of ivacaftor (50 nM), respectively. Values are means ± SD of *n* observations. Measurements were made at 37 °C in the absence and presence of ivacaftor (50 nM) in the intracellular solution; the catalytic subunit of PKA (75 nM) and ATP (1 mM) were continuously present in the intracellular solution, voltage was –50 mV and there was a large Cl^- concentration gradient across the membrane patch ($[Cl^-]_{int}$, 147 mM; $[Cl^-]_{ext}$, 10 mM).

FIGURE LEGENDS

Figure 1. Structure of human CFTR showing the rare variants at codon S1159 in the twelfth transmembrane segment *A*, orthogonal views of PyMOL representations of a 3D model of phosphorylated, ATP-bound wild-type human CFTR complexed with ivacaftor (based on PDB id: 6O2P). The lefthand image shows the ivacaftor-binding site, while the righthand image has been rotated 180° to reveal the position of S1159 (see dashed box). The twelfth transmembrane segment (M12) is coloured wheat and M9 light blue. The R domain, unresolved in cryo-EM structures of CFTR (e.g. Liu *et al*., 2019), has been omitted. The position of the plasma membrane is shown with the intracellular (In) and extracellular (Out) sides indicated. The chemical structures of ATP and ivacaftor are displayed in green and magenta, respectively. *B*–*D*, magnified views of the regions of M9 and M12 enclosed by the dashed box in *A* to show the interactions of D979 (pink) (M9) with S1159 (white), S1159F (red) and S1159P (orange). The hydrogen bond between S1159 and D979 is indicated by a yellow dashed line, with a bond length of 1.7 Å.

Figure 2. The multi-channel behaviour of S1159-*CFTR* variants Representative multi-channel recordings and corresponding current amplitude histograms of wild-type (*A*), S1159F- (*B*) and S1159P-CFTR (*C*) in excised inside-out membrane patches from transiently transfected CHO-K1 cells. ATP (1 mM) and PKA (75 nM) were continuously present in the intracellular solution. Dotted lines indicate the closed channel state, arrowheads identify different open channel current levels and downward deflections correspond to channel openings. The labels C and O1 – O4 denote the closed and open channel amplitudes, respectively. Because openings of the S1159-*CFTR* variants to O3 and O4 were rare, they are not apparent in the current amplitude histograms. Unless otherwise indicated in this and subsequent figures, membrane voltage was clamped at –50 mV, a large Cl^- concentration gradient was imposed across the membrane patch ($[Cl^-]_{int}$, 147 mM; $[Cl^-]_{ext}$, 10 mM) and temperature was 37 °C.

Figure 3. The single-channel behaviour of S1159-*CFTR* variants *A*, representative single-channel recordings and corresponding current amplitude histograms of wild-type, S1159F- and S1159P-CFTR in excised inside-out membrane patches from transiently transfected CHO-K1 cells. ATP (1 mM) and PKA (75 nM) were continuously present in the intracellular solution. Dotted lines indicate the closed channel state and downward deflections correspond to channel openings. The labels C and O denote the closed and open channel amplitudes,

respectively. *B–E*, summary single-channel current amplitude (*i*), interburst interval (*IBI*), mean burst duration (*MBD*) and open probability (P_o) data determined from prolonged recordings (≥ 4 min) of wild-type, S1159F- and S1159P-CFTR for the experimental conditions described in *A*. Symbols represent individual values and columns represent means ± SD (wild-type: *i* and P_o, *n* = 15; *MBD* and *IBI*, *n* = 8; S1159F: *i* and P_o, *n* = 22; *MBD* and *IBI*, *n* = 15; S1159P: *i* and P_o, *n* = 24; *MBD* and *IBI*, *n* = 13). [Panel *B*: ***$P < 0.001$ vs. wild-type CFTR; one-way ANOVA with Tukey post-hoc test; normality test (Shapiro–Wilk), $P < 0.050$ (failed); equal variance test (Brown-Forsythe), $P = 0.350$ (passed). Panel *C*: *$P = 0.013$ and **$P = 0.001$ vs. wild-type CFTR; Kruskal-Wallis one-way ANOVA on Ranks with Dunn's post-hoc test; normality test (Shapiro–Wilk), $P < 0.050$ (failed). Panel *D*: ***$P < 0.001$ vs. wild-type CFTR; one-way ANOVA with Tukey post-hoc test; normality test (Shapiro–Wilk), $P = 0.620$ (passed); equal variance test (Brown-Forsythe), $P = 0.050$ (passed). Panel *E*: ***$P < 0.001$ vs. wild-type CFTR; one-way ANOVA with Tukey post-hoc test; normality test (Shapiro–Wilk), $P = 0.490$ (passed); equal variance test (Brown-Forsythe), $P < 0.050$ (failed)].

Figure 4. Impact of S1159-*CFTR* variants on the single-channel conductance of CFTR *A*, representative single-channel recordings of wild-type, S1159F- and S1159P-CFTR in excised inside-out membrane patches from transiently transfected CHO-K1 cells acquired at the indicated voltages. ATP (1 mM) and PKA (75 nM) were continuously present in the intracellular solution. Dotted lines indicate the closed channel state and downward deflections correspond to channel openings. *B* and *C*, single-channel current-voltage (*i–V*) relationships and summary slope conductance data of wild-type, S1159F- and S1159P-CFTR. Data are means ± SD (wild-type, *n* = 11–14; S1159F-CFTR, *n* = 3–5; S1159P-CFTR, *n* = 7–9). In *B*, the continuous lines are the fit of first order linear regression functions to mean data ($r^2 > 0.99$), while in *C*, symbols represent individual values.

Figure 5. Dwell time histograms of S1159-*CFTR* variants Representative dwell time histograms of wild-type (*A*), S1159F- (*B*) and S1159P-CFTR (*C*). Data are from experiments in which the excised inside-out membrane patch from transiently transfected CHO-K1 cells (*B* and *C*) [or stably transfected C127 cells (*A*)] contained only one active channel, studied in the presence of ATP (1 mM) and PKA (75 nM) in the intracellular solution; membrane voltage was –50 mV, a large Cl^- concentration gradient was imposed across the membrane patch ($[Cl^-]_{int}$, 147 mM; $[Cl^-]_{ext}$, 10 mM) and temperature was 37 °C. The continuous lines are

the fit of one- or two-component exponential functions to the data and the dotted lines show the individual components of these functions. The vertical dashed lines indicate the mean values of the open (τ_{O2}) and closed (τ_{C1}, τ_{C3}) time constants. Logarithmic x-axes with 10 bins decade^{-1} were used for dwell time histograms.

Figure 6. Impact of S1159-*CFTR* variants on the ATP-dependent channel gating of CFTR *A*, representative single-channel recordings of wild-type-, S1159F- and S1159P-CFTR in excised inside-out membrane patches from transiently transfected CHO-K1 cells acquired using the indicated intracellular ATP concentrations. PKA (75 nM) was continuously present in the intracellular solution. Dotted lines indicate the closed channel state and downward deflections correspond to channel openings. *B–D*, relationship between ATP concentration and open probability (P_o), mean burst duration (*MBD*) and interburst interval (*IBI*) for wild-type and S1159-*CFTR* variants; note that in *D*, the y-axis is plotted using a logarithmic scale. Data are means ± SD (wild-type: P_o, n = 11–23; *MBD* and *IBI*, n = 6–8; S1159F: P_o, n = 2–22; *MBD* and *IBI*, n = 2–15; S1159P: P_o, S1159P, n = 11–24; *MBD* and *IBI*, n = 7–13) from experiments where ≥ 3 ATP concentrations were tested in each membrane patch. In *B*, the continuous lines are the fit of Michaelis–Menten functions to mean data ($r^2 \geq 0.93$).

Figure 7. Ivacaftor potentiates the channel gating of S1159-*CFTR* variants, but inhibits current flow through S1159F-CFTR *A*, representative single-channel recordings of S1159F- and S1159P-CFTR in excised inside-out membrane patches from transiently transfected CHO-K1 cells in the absence and presence of ivacaftor. Ivacaftor (VX-770, 50 and 500 nM) was acutely added to the intracellular solution in the continuous presence of ATP (1 mM) and PKA (75 nM). Dotted lines indicate the closed channel state, downward deflections correspond to channel openings and teal is used to identify single-channel recordings acquired at a supersaturated concentration of ivacaftor. *B* and *C*, relationships between ivacaftor concentration and single-channel open probability (P_o) and current amplitude (i) for S1159-*CFTR* variants at –50 mV. Data are means ± SD (S1159F, n = 3–5; S1159P, n = 8–9). *D* and *E*, single-channel current-voltage (i–V) relationships of S1159F- and S1159P-CFTR in the absence and presence of ivacaftor (50 and 500 nM) in the intracellular solution. Data are means ± SD (S1159F: n = 2–3; S1159P: n = 2–4). In *B–E*, triangles indicate supersaturated concentrations of ivacaftor. In *C–E*, the continuous lines are

the fit of first order linear regression functions to mean data (*C*, $r^2 > 0.90$; *D* and *E*, $r^2 > 0.98$), whereas in *B*, they are the fit of peak log normal functions to mean data.

Figure 8. Effects of ivacaftor on the single-channel behaviour of wild-type and S1159F-CFTR at different membrane voltages *A* and *B*, representative single-channel recordings and corresponding current amplitude histograms of wild-type and S1159F-CFTR in excised inside-out membrane patches from CFTR-expressing C127 and CHO cells, respectively. The recordings were acquired at ±50 mV in the absence and presence of ivacaftor (VX-770; 100 and 1000 nM). Membrane patches were bathed in symmetrical 147 mM Cl^- solutions, ATP (1 mM) and PKA (75 nM) were continuously present in the intracellular solution and temperature was 37 °C. Dotted lines indicate the closed channel state and downward deflections at –50 mV and upward deflections at +50 mV correspond to channel openings. The labels C and O denote the closed and open channel amplitudes, respectively. In *A* and *B*, teal is used to identify single-channel recordings and current amplitude histograms acquired at a supersaturated concentration of ivacaftor. For ivacaftor (100 and 1000 nM), small leak currents at +50 mV shifted the current amplitude histograms of S1159F-CFTR by ~ 0.2 pA and 1.8 pA relative to that of the control. For summary single-channel current-voltage (*i*–*V*) and open probability-voltage (P_o–*V*) relationships of wild-type and S1159F-CFTR, see Figure 10.

Figure 9. Actions of ivacaftor (50 nM) on the dwell time histograms of S1159F-CFTR Representative dwell time histograms of S1159F-CFTR in the absence (*A*) and presence (*B*) of ivacaftor (VX-770, 50 nM). Data are from experiments in which the excised inside-out membrane patch from transiently transfected CHO-K1 cells contained only one active channel, studied in the presence of ATP (1 mM) and PKA (75 nM) in the intracellular solution; membrane voltage was –50 mV, a large Cl^- concentration gradient was imposed across the membrane patch ($[Cl^-]_{int}$, 147 mM; $[Cl^-]_{ext}$, 10 mM) and temperature was 37 °C. The continuous lines are the fit of one- or two-component exponential functions to the data and the dotted lines show the individual components of these functions. The black vertical dashed lines indicate the mean values of the open (τ_{O2}) and closed (τ_{C1}, τ_{C3}) time constants of S1159F-CFTR, while the grey vertical dotted lines indicate the same values for wild-type CFTR in the absence of ivacaftor. Logarithmic x-axes with 10 bins $decade^{-1}$ were used for dwell time histograms.

Figure 10. Ivacaftor inhibition of current flow through S1159F-CFTR is voltage-independent Single-channel open probability-voltage (P_o–V) relationships (*A*, *D*), current-voltage (*i*–*V*) relationships (*B*, *E*) and summary slope conductance data (*C*, *F*) for wild-type (*A* – *C*) and S1159F-CFTR (*D* – *F*) in the absence and presence of ivacaftor (VX-770; 100 and 1000 nM). The data were acquired using excised inside-out membrane patches from C127 and CHO cells heterologously expressing wild-type and S1159F-CFTR, respectively, using the experimental conditions described in Figure 8. Data are means ± SD (wild-type, n = 5; S1159F, n = 4–6). In *A*, *B*, *D* and *E*, triangles indicate supersaturated concentrations of ivacaftor, while in *C* and *F*, these concentrations are identified by hatching. [Panel *A*, wild-type CFTR: ***P < 0.001 vs. control at ±50 mV; one-way ANOVA with Tukey post-hoc test; normality test (Shapiro–Wilk), P = 0.491 (passed); equal variance test (Brown-Forsythe), P < 0.050 (failed); †P = 0.0316 (two-tailed) vs. 100 nM VX-770 at –50 mV; Student's paired t-test; normality test (Shapiro–Wilk), P = 0.524 (passed); †P = 0.0131 (two-tailed) vs. 100 nM VX-770 at +50 mV; Student's paired t-test; normality test (Shapiro–Wilk), P = 0.557 (passed). Panel *D*, S1159F: **P = 0.003 vs. control at ±50 mV; one-way ANOVA with Tukey post-hoc test; normality test (Shapiro–Wilk), P = 0.271 (passed); equal variance test (Brown-Forsythe), P = 0.065 (passed). Panels *B* and *E*: the continuous lines are the fit of second order regression functions to mean data ($r^2 \geq 0.98$). Panel *F*, S1159F: ***P < 0.001 vs. control; †††P < 0.001 vs 100 nM VX-770; one-way ANOVA with Tukey post-hoc test; normality test (Shapiro–Wilk), P = 0.939 (passed); equal variance test (Brown-Forsythe), P = 0.739 (passed)].

Abstract Figure: This study investigated two rare cystic fibrosis transmembrane conductance regulator (*CFTR*) variants, S1159F and S1159P, which affect the same amino acid in CFTR by breaking a hydrogen bond (dotted line) with D979, that are associated with different disease phenotypes. S1159P appears to be associated with residual exocrine pancreatic function (pancreatic sufficiency) and S1159F with loss of exocrine pancreatic function (pancreatic insufficiency). Using single-channel recording in cell-free membrane patches (the dotted lines indicate where channels are closed and downward deflections correspond to channel openings), both rare variants modestly reduced current flow through CFTR, but markedly inhibited channel gating with S1159F causing the severer impact, which correlates with its disease phenotype. Thus, detailed CFTR investigations explain phenotypic differences, informing treatment with CFTR-targeted therapies.

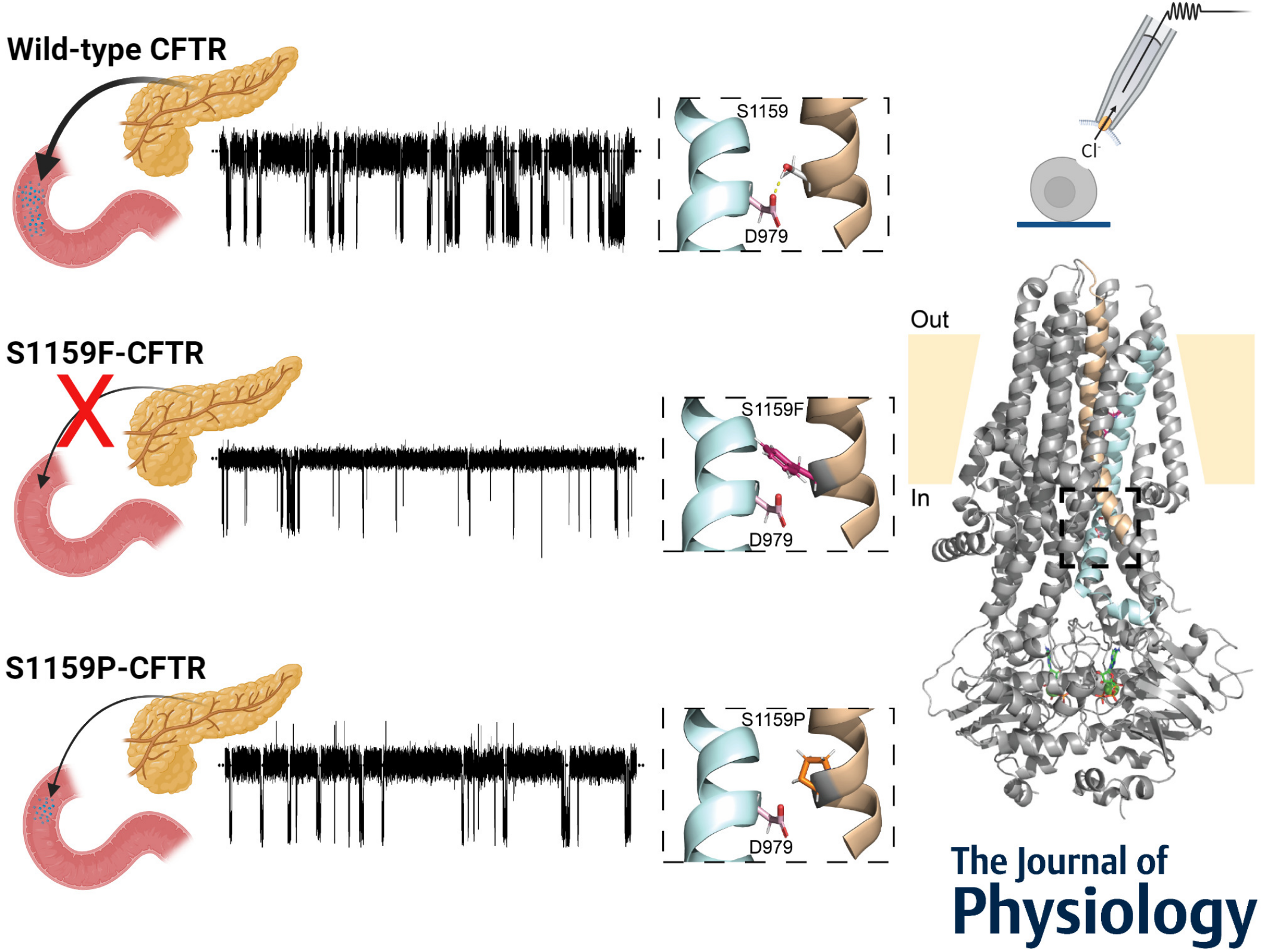
Wild-type CFTR
S1159
D979
Cl-
S1159F-CFTR
S1159F
D979
Out
In
S1159P-CFTR
S1159P
D979
The Journal of
Physiology

Figure 1

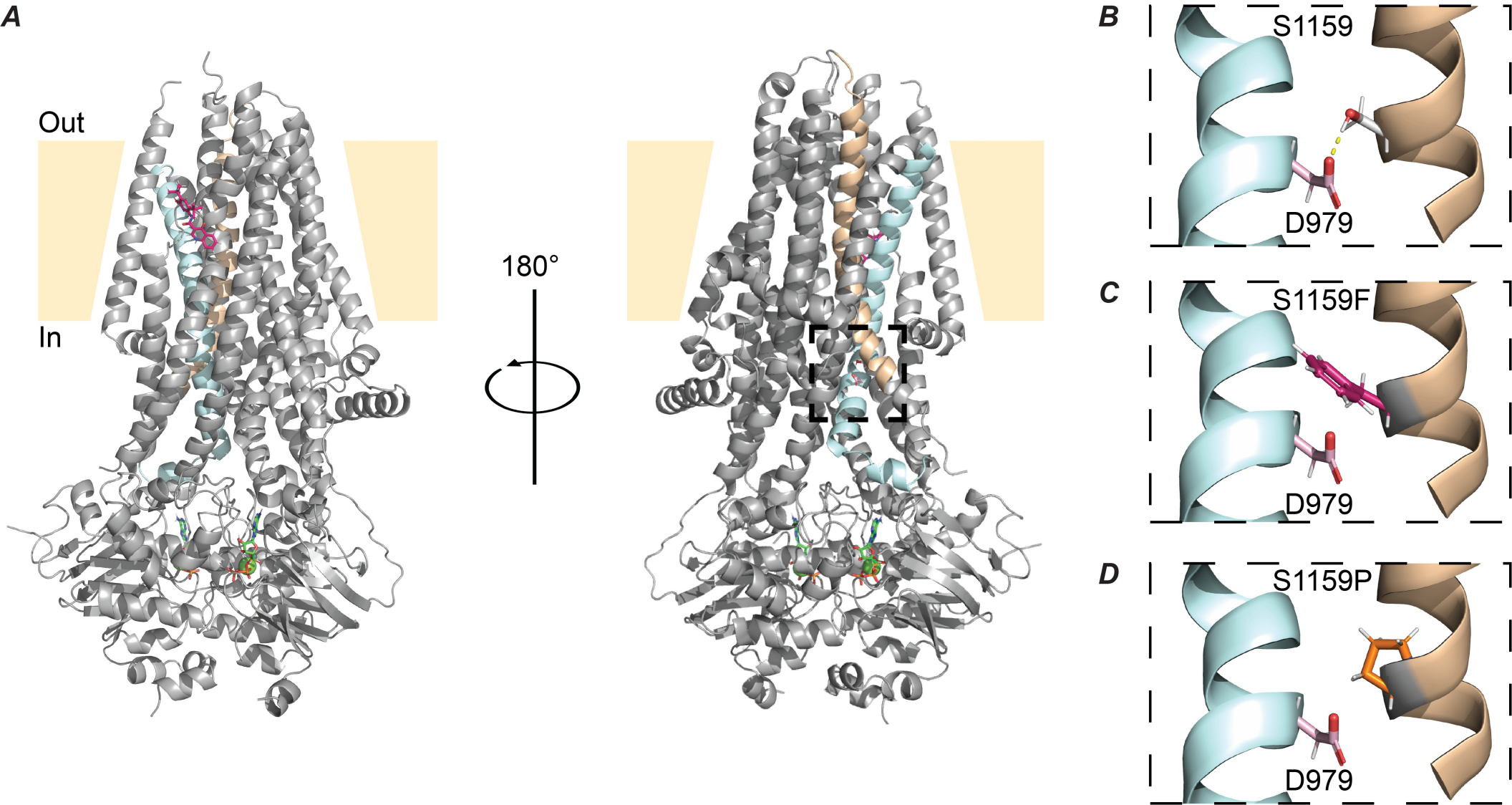

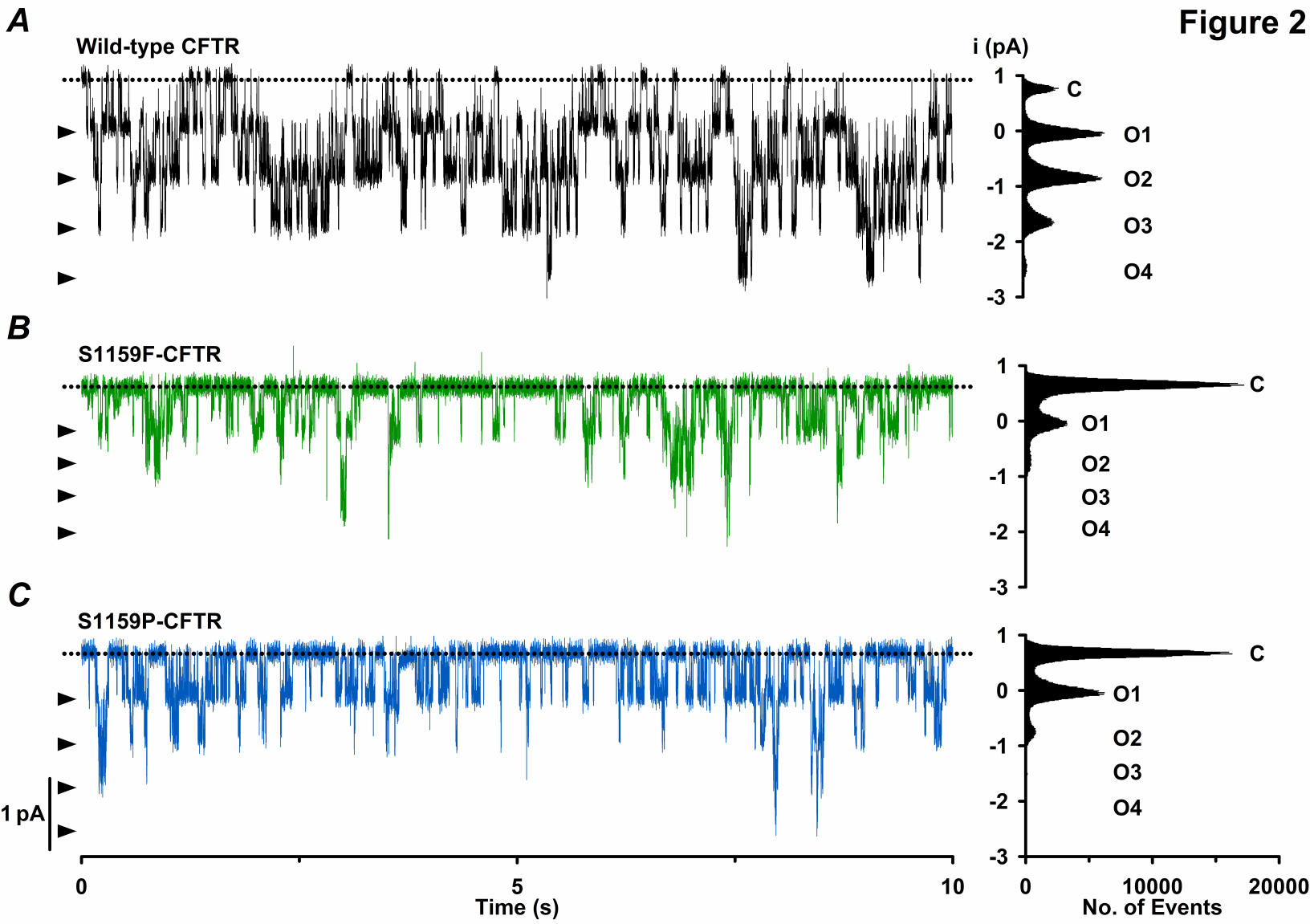
A
Wild-type CFTR
i (pA)
1
0
-1
-2
-3
C
O1
O2
O3
O4
B
S1159F-CFTR
C
O1
O2
O3
O4
C
S1159P-CFTR
C
O1
O2
O3
O4
1 pA
0
5
10
Time (s)
0
10000
20000
No. of Events

Figure 2

Figure 3

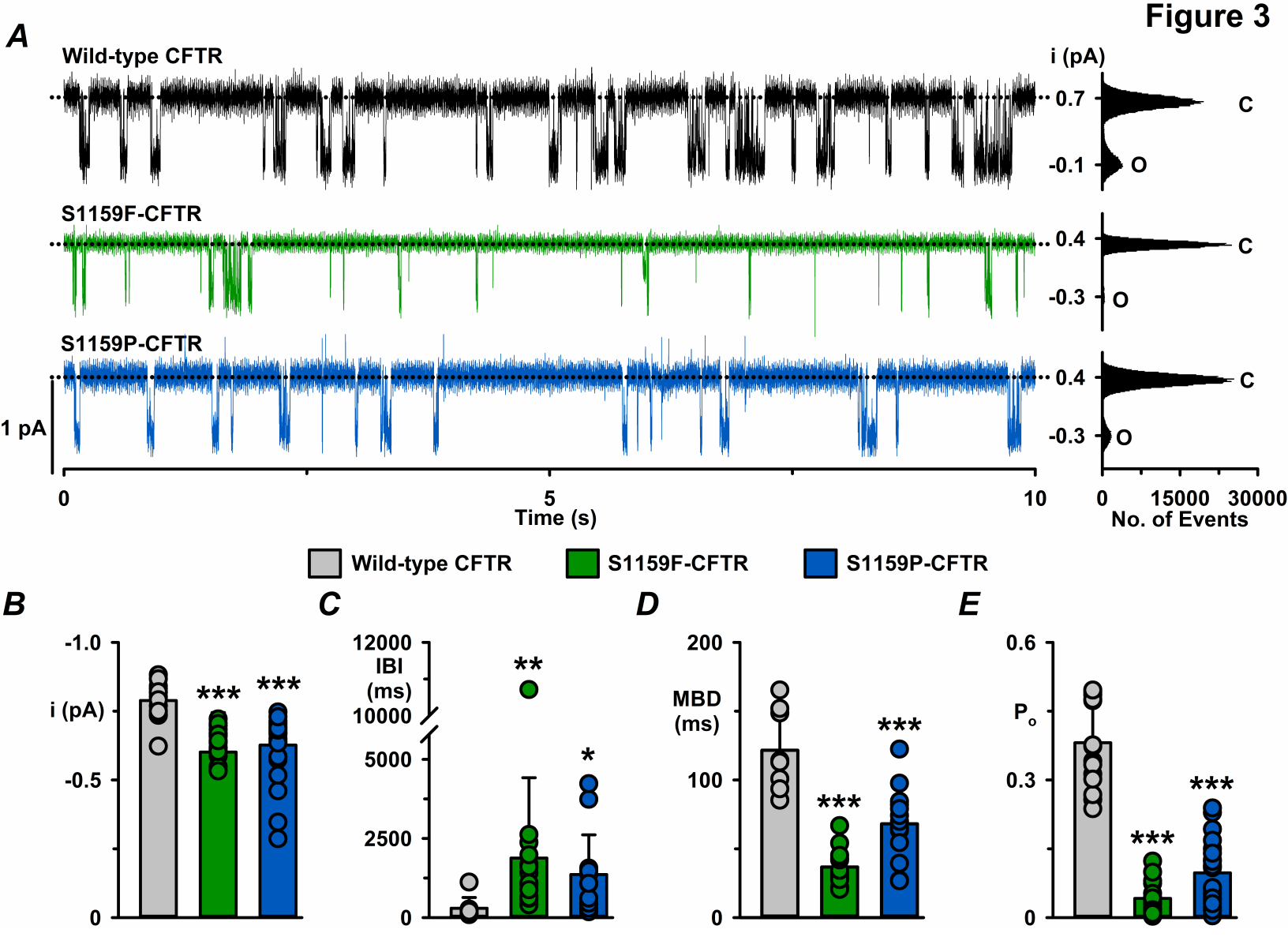
A
Wild-type CFTR
S1159F-CFTR
S1159P-CFTR
i (pA)
0.7
-0.1
0.4
-0.3
0.4
-0.3
C
O
1 pA
0
5
10
Time (s)
0
15000
30000
No. of Events
Wild-type CFTR
S1159F-CFTR
S1159P-CFTR
B
-1.0
i (pA)
-0.5
0
***
***
C
12000
IBI
(ms)
10000
5000
2500
0
**
*
D
200
MBD
(ms)
100
0
***
***
E
0.6
Po
0.3
0
***
***

Figure 4

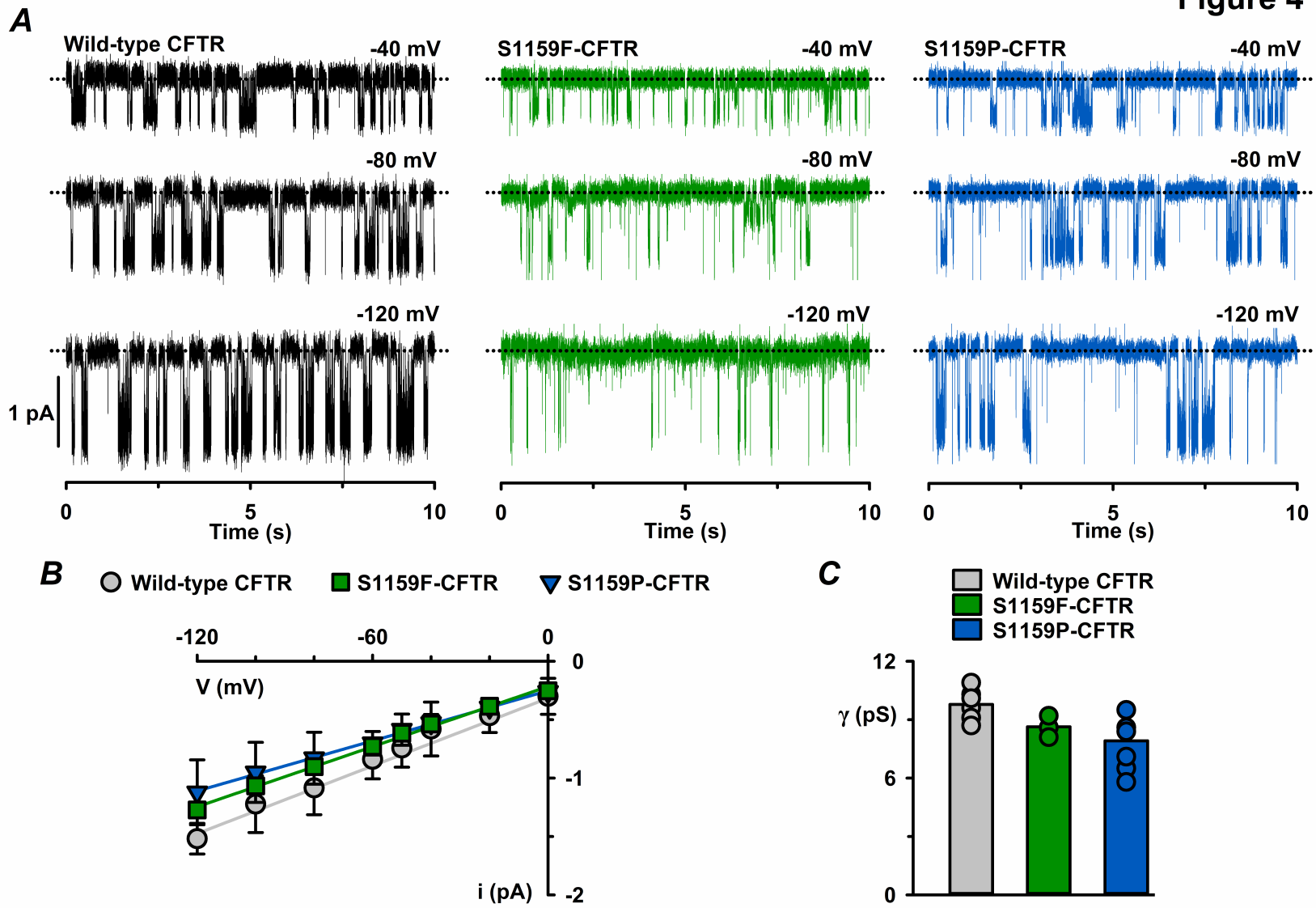
A
Wild-type CFTR
S1159F-CFTR
S1159P-CFTR
-40 mV
-80 mV
-120 mV
1 pA
0
5
10
Time (s)
B
Wild-type CFTR
S1159F-CFTR
S1159P-CFTR
-120
-60
0
V (mV)
0
-1
-2
i (pA)
C
Wild-type CFTR
S1159F-CFTR
S1159P-CFTR
12
6
0
γ (pS)

Figure 5

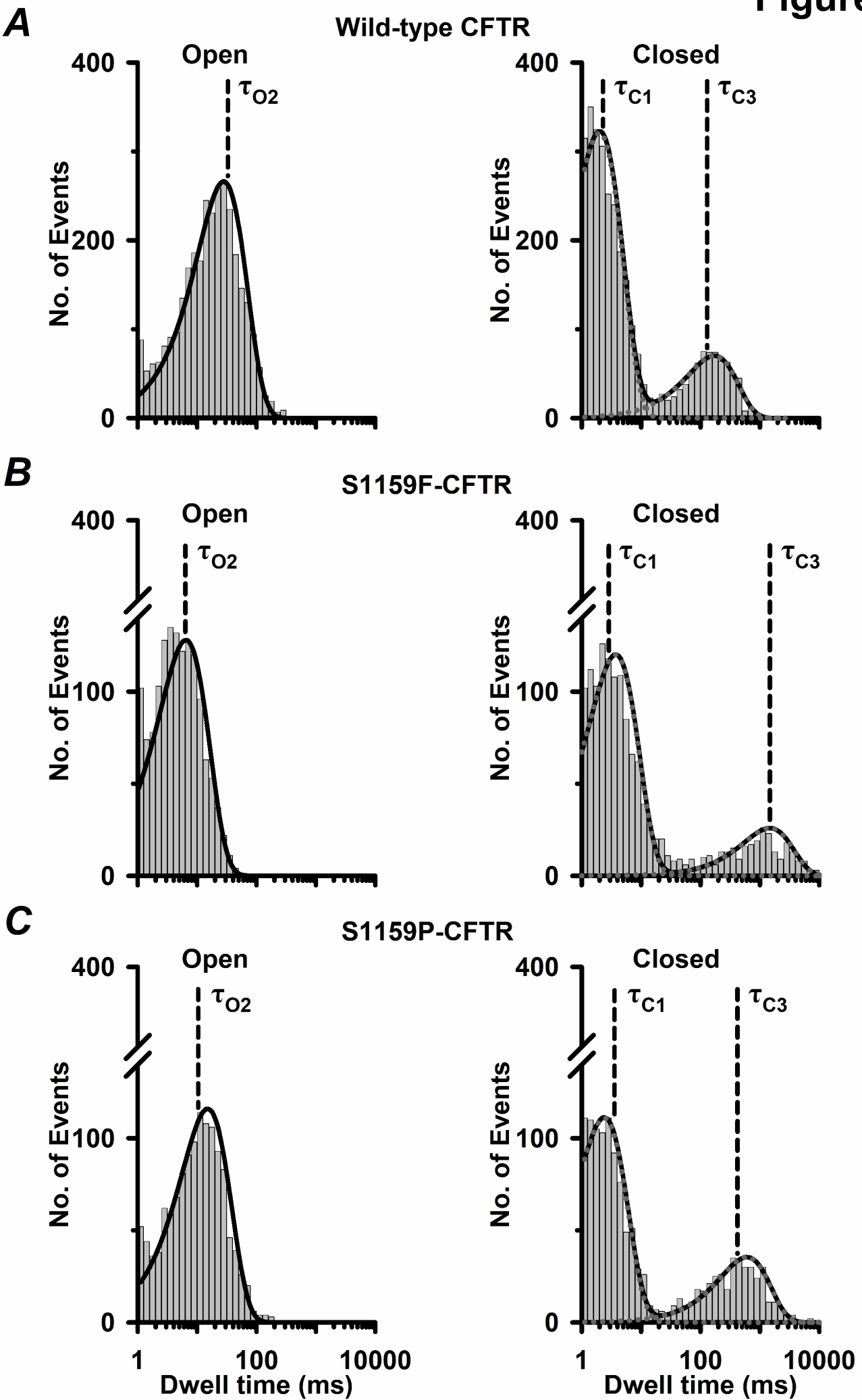
A
Wild-type CFTR
Open
Closed
τ_{O2}
τ_{C1}
τ_{C3}
No. of Events
400
200
0
B
S1159F-CFTR
Open
Closed
τ_{O2}
τ_{C1}
τ_{C3}
No. of Events
400
100
0
C
S1159P-CFTR
Open
Closed
τ_{O2}
τ_{C1}
τ_{C3}
No. of Events
400
100
0
1
100
10000
Dwell time (ms)

Figure 6

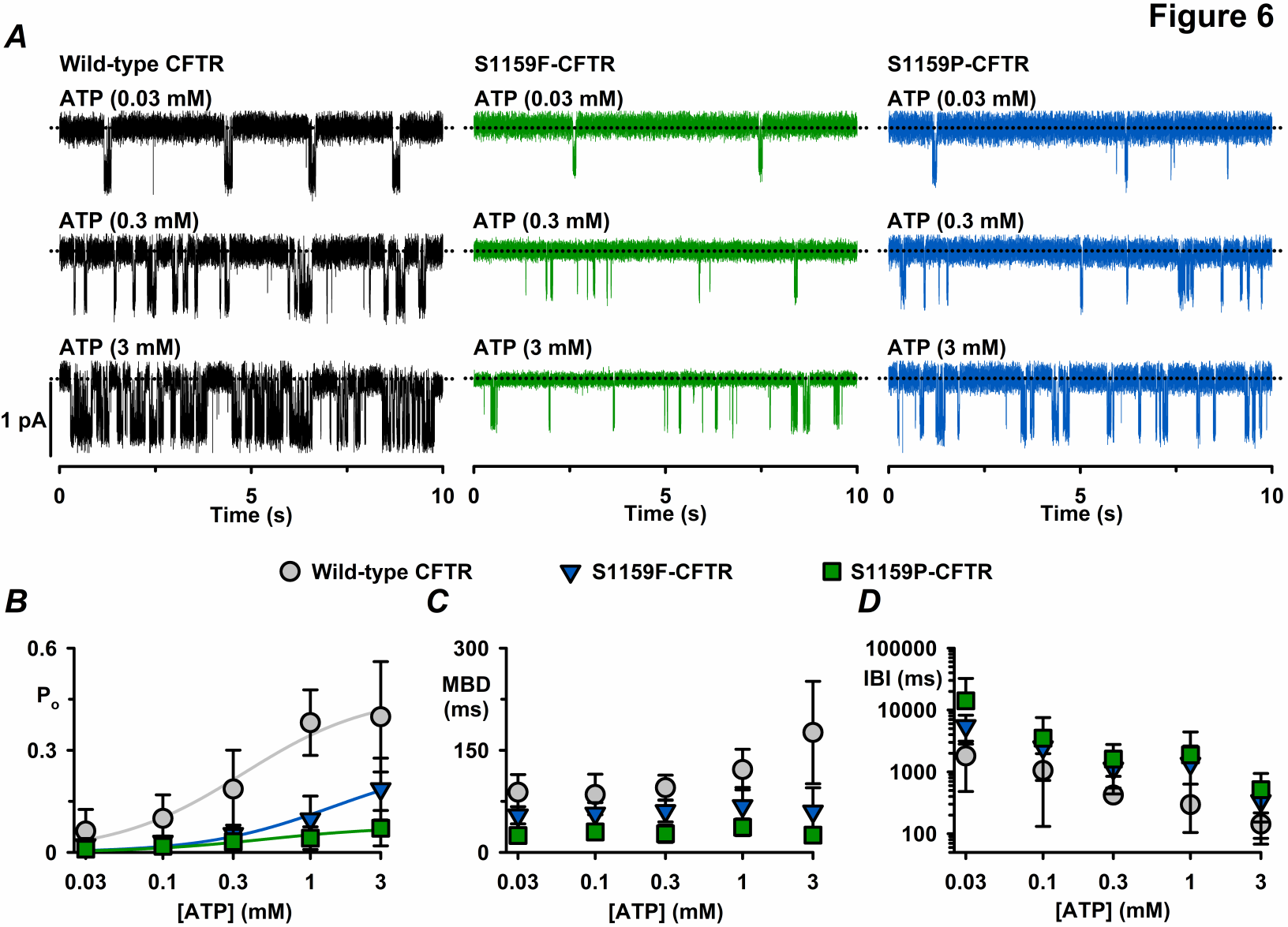
A
Wild-type CFTR
S1159F-CFTR
S1159P-CFTR
ATP (0.03 mM)
ATP (0.3 mM)
ATP (3 mM)
1 pA
0
5
10
Time (s)
Wild-type CFTR
S1159F-CFTR
S1159P-CFTR
B
C
D
0.6
Po
0.3
0
0.03
0.1
0.3
1
3
[ATP] (mM)
300
MBD
(ms)
150
100000
IBI (ms)
10000
1000
100

Figure 7

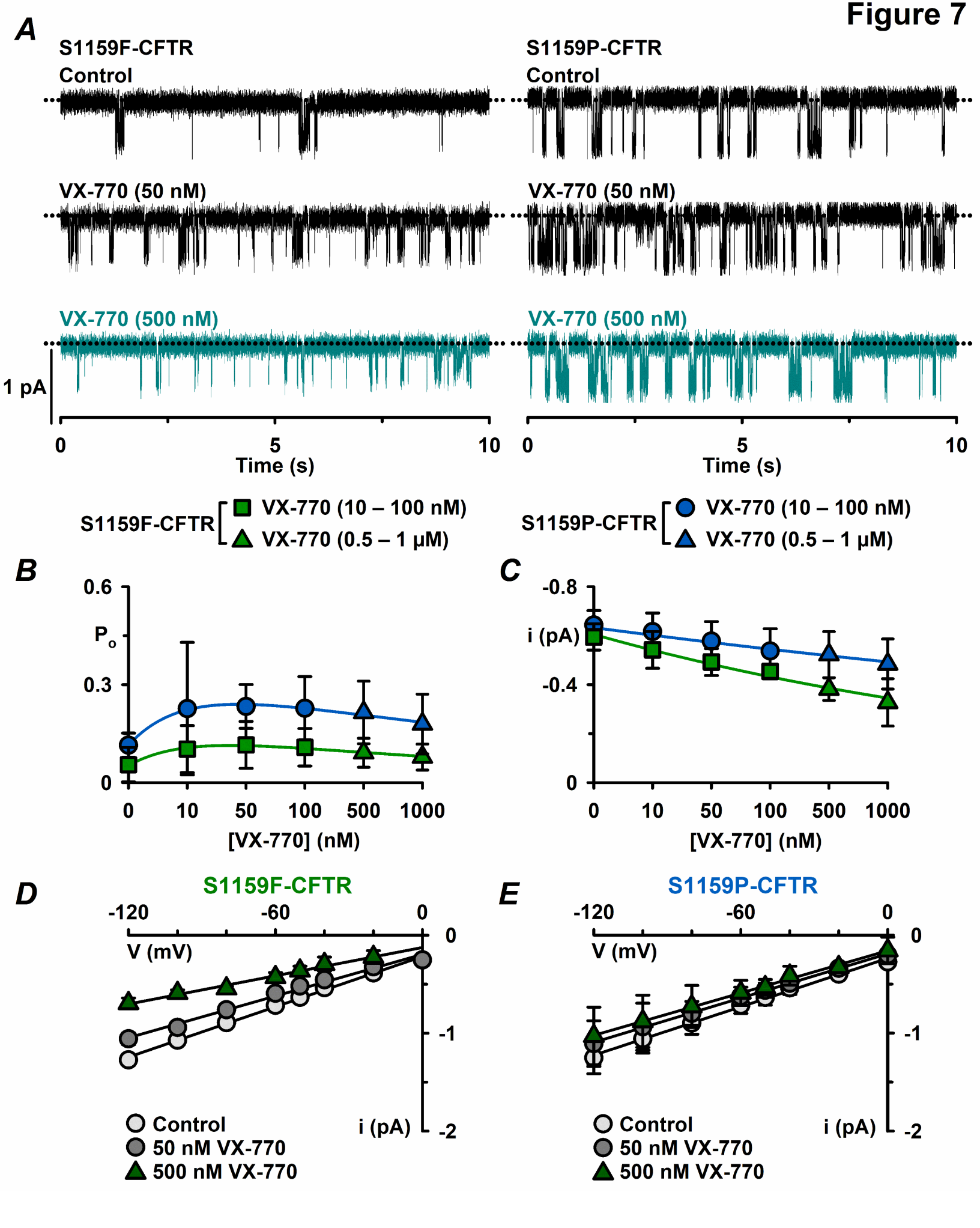
A
S1159F-CFTR
Control
VX-770 (50 nM)
VX-770 (500 nM)
1 pA
0
5
10
Time (s)
S1159P-CFTR
Control
VX-770 (50 nM)
VX-770 (500 nM)
0
5
10
Time (s)
S1159F-CFTR
VX-770 (10 – 100 nM)
VX-770 (0.5 – 1 μM)
S1159P-CFTR
VX-770 (10 – 100 nM)
VX-770 (0.5 – 1 μM)
B
0.6
P$_o$
0.3
0
0
10
50
100
500
1000
[VX-770] (nM)
C
-0.8
i (pA)
-0.4
0
0
10
50
100
500
1000
[VX-770] (nM)
D
S1159F-CFTR
-120
-60
0
V (mV)
0
-1
-2
i (pA)
Control
50 nM VX-770
500 nM VX-770
E
S1159P-CFTR
-120
-60
0
V (mV)
0
-1
-2
i (pA)
Control
50 nM VX-770
500 nM VX-770

Figure 8

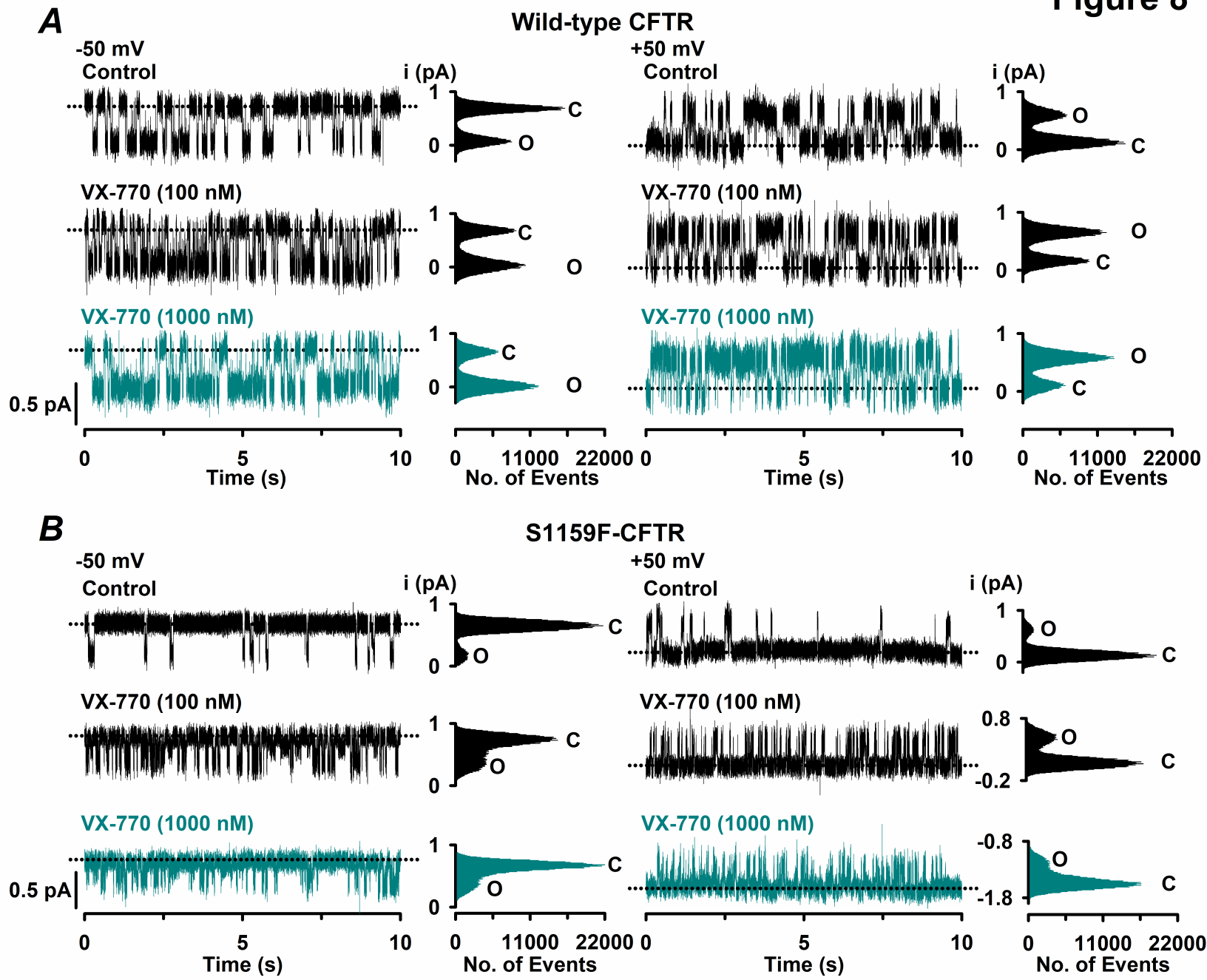
A
Wild-type CFTR
-50 mV
Control
i (pA)
1
0
C
O
VX-770 (100 nM)
VX-770 (1000 nM)
0.5 pA
0
5
10
Time (s)
0
11000
22000
No. of Events
+50 mV
B
S1159F-CFTR
0.8
-0.2
-0.8
-1.8

Figure 9

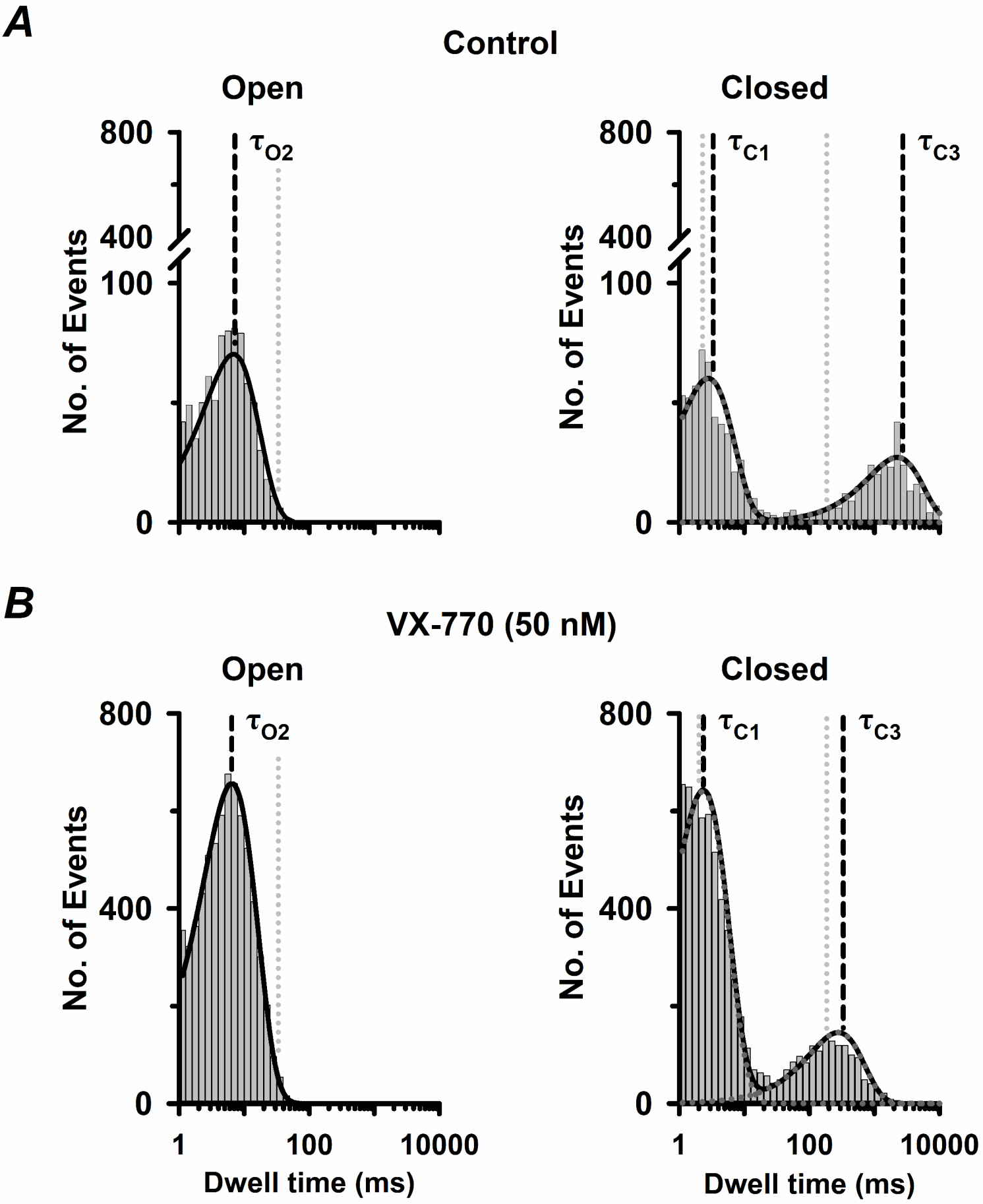
A
Control
Open
Closed
800
400
100
0
No. of Events
τ_{O2}
τ_{C1}
τ_{C3}
B
VX-770 (50 nM)
Open
Closed
800
400
0
No. of Events
τ_{O2}
τ_{C1}
τ_{C3}
1
100
10000
Dwell time (ms)

Figure 10

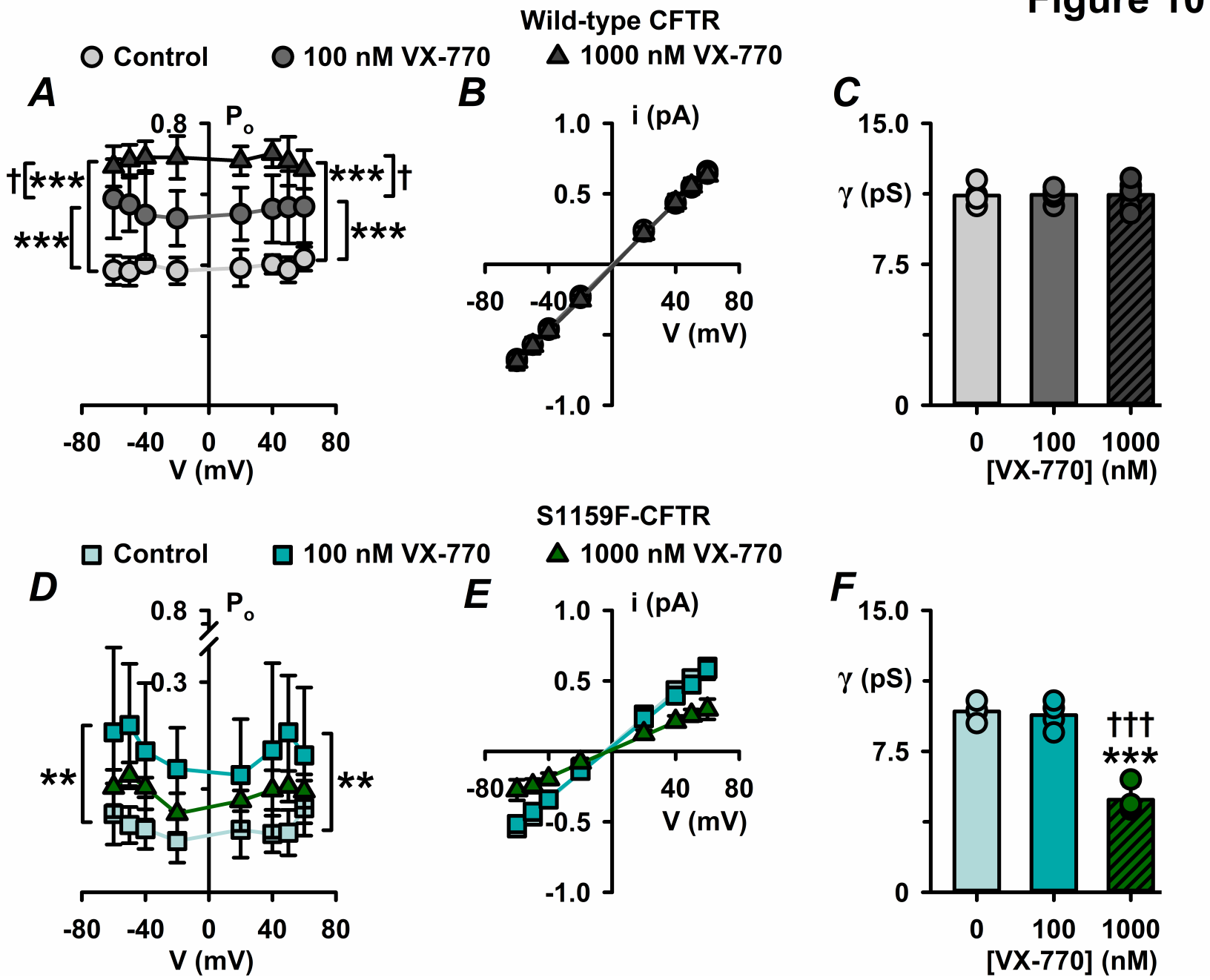
Wild-type CFTR
Control
100 nM VX-770
1000 nM VX-770
A
B
C
0.8
P_o
†[***
***]†
***[
]***
-80
-40
0
40
80
V (mV)
1.0
i (pA)
0.5
-1.0
15.0
γ (pS)
7.5
0
100
1000
[VX-770] (nM)
S1159F-CFTR
Control
100 nM VX-770
1000 nM VX-770
D
E
F
0.3
**[
]**
-0.5
†††
***